6-8-2018

Formation Control of Nonholonomic Multi-Agent Systems

Milad Khaledyan
Louisiana State University and Agricultural and Mechanical College

FORMATION CONTROL OF NONHOLONOMIC MULTI-AGENT SYSTEMS

A Dissertation

Submitted to the Graduate Faculty of the
Louisiana State University and
Agricultural and Mechanical College
in partial fulfillment of the
requirements for the degree of
Doctor of Philosophy

in

The Department of Mechanical and Industrial Engineering

by
Milad Khaledyan
B.S., Aerospace Engineering, Sharif University of Technology, Iran, 2014
August 2018

To my beloved parents,
Farideh and Mozafar

Acknowledgments

I would like to deeply thank my advisor, Dr. Marcio de Queiroz, for all his support, guidance, knowledge and patience through last four years. Without his continuous support and effort, this dissertation would not be possible. I would also express my appreciation to Dr. Wanjun Wang and Dr. Hunter Gilbert for serving on my doctoral examination committee.

I am very thankful to the department of Mechanical Engineering for providing me the financial support through these years and giving me the opportunity to serve as instructor for several courses.

I would like to thank my parents, and my siblings, Donya, Somayeh, Shaho, Shahab, and Mehrdad for being there whenever I needed it. Their supports, encouragements, and patience have enlightened my path toward completing my studies.

Finally, I want to thank my colleagues and my friends who supported me all along the way.

Table of Contents

List of Figures

Abstract

This dissertation is concerned with the formation control problem of multiple agents modeled as nonholonomic wheeled mobile robots. Both kinematic and dynamic robot models are considered. Solutions are presented for a class of formation problems that include formation, maneuvering, and flocking. Graph theory and nonlinear systems theory are the key tools used in the design and stability analysis of the proposed control schemes. Simulation and/or experimental results are presented to illustrate the performance of the controllers.

In the first part, we present a leader-follower type solution to the formation maneuvering problem. The solution is based on the graph that models the coordination among the robots being a spanning tree. Our control law incorporates two types of position errors: individual tracking errors and coordination errors for leader-follower pairs in the spanning tree. The control ensures that the robots globally acquire a given planar formation while the formation as a whole globally tracks a desired trajectory, both with uniformly ultimately bounded errors. The control law is first designed at the kinematic level and then extended to the dynamic level. In the latter, we consider that parametric uncertainty exists in the equations of motion. These uncertainties are accounted for by employing an adaptive control scheme.

In the second part, we design a distance-based control scheme for the flocking of the nonholonomic agents under the assumption that the desired flocking velocity is known to all agents. The control law is designed at the kinematic level and is based on the rigidity properties of the graph modeling the sensing/control interactions among the robots. A simple input transformation is used to facilitate the control design by converting the nonholonomic model into the single-integrator equation. The resulting control ensures exponential convergence to the desired formation while the formation maneuvers according to a desired, time-varying translational velocity.

In the third part, we extend the previous flocking control framework to the case where only a subset of the agents know the desired flocking velocity. The resulting controllers include distributed observers to estimate the unknown quantities. The theory of interconnected systems is used to analyze the stability of the observer-controller system.

Chapter 1. Introduction

1.1 Motivation

The exotic collective behavior of natural swarming species such as schools of fish, colonies of ants, bee colonies, flocks of birds, and groups of insects has attracted the attention of many systems and control researchers for the past decades. Collaborative behaviors serve needs such as survival, defense against predators, and foraging for food. With this inspiration and the development in technologies such as sensors, embedded systems, communication systems, and power storage, it has become feasible to tackle problems such as surveillance, exploration, rescue missions, mapping and environmental monitoring, by deploying formations of robotic vehicles.

A *multi-agent system* refers to the coordinated behavior of multiple, interacting physical entities as they perform tasks unsuitable and/or too complex for a single entity. For variety of reasons, using multi-agent systems is more effective than deploying single vehicles to accomplish a task: more efficient and complex task execution, versatility, adaptability, scalability, lower cost, and robustness when one or more robots fail. For example, multiple robots could use its neighbors' relative positions to synthesize a virtual, large scale antenna to receive acoustic signals with better sensitivity. If one of the robots fails, the rest can reconfigure to maintain the antenna operational, whereas a stand-alone antenna would be a single point of failure. Roughly speaking, malfunctions in multi-agent systems are less likely than a single agent since they are usually much simpler hardware- and software-wise. This simplicity along with mass production can also lead to lower costs. Another application that can benefit form the use of multi-agent system is the survey of large geographic areas since multiple robot sensors can cover the region of interest more rapidly than a single one. Lastly, multiple robots with on-board sensors may have different functionalities, which may give the whole formation a new functionality in the aggregate. For instance, in a group of underwater vehicles, some could be equipped with sonar sensors and others with radio-frequency direction sensors to allow target identification and localization by the entire formation [1].

The multi-agent system concept, on the other hand, introduces a list of unique challenges such as communication topology, control protocols, collision avoidance, information exchange, and

cooperation and coordination algorithms. These challenges are often complicated by restrictions on computational, communication, and sensing resources. A key design decision is choosing between a centralized coordination scheme (e.g., GPS or a central command station) or decentralized/distributed one (local/on-board sensors and processing). A decentralized scheme is typically the preferred approach since it maximizes the benefits of the multi-agent system concept.

Numerous collaborative and coordination problems for multi-agent systems have been studied over the past decade: foraging, consensus, formation, coverage, flocking, rendezvous, agreement, scheduling, and synchronization. The aim of these problems is mostly to drive the multi-agent system to a common state such as velocity, position, planar or spatial formations, arrival time, etc. In this dissertation, we will mainly focus on the class of formation problems. *Formation acquisition* is the most basic formation control problem, and refers to the coordinated behavior where mobile agents are required to autonomously configure into a desired spatial pattern. *Formation maneuvering* refers to the special case where the formation is not static, but moves in space as a virtual rigid body according to a pre-defined trajectory. *Flocking* is a type of formation maneuvering where the trajectory is described by a desired translational velocity. Notice that formation acquisition is a pre-condition for the other problems.

1.2 Literature Review and Scope of Work

Most formation control results are based on point-mass type models for the agent's motion, such as the single- and double-integrator models. For example, see [11, 29, 34, 45, 57, 66, 69, 76] for single-integrator results and [10, 13, 34, 56, 58] for double-integrator results. On the other hand, some results have used more sophisticated models that account for the agent kinematics/dynamics. One of two models are used in these cases: the fully-actuated (holonomic) Euler-Lagrange model, which includes robot manipulators, spacecraft, and some omnidirectional mobile robots; or the nonholonomic (underactuated) model, which accounts for velocity constraints that typically occur in the vehicle motion (e.g., wheeled mobile robots and air vehicles). In the nonholonomic case, models can be further subdivided into two categories: the purely kinematic model where the control inputs are at the velocity level, and the dynamic model where the inputs are at the actuator level.

Examples of work based on the Euler-Lagrange model include [12, 16, 19, 26, 41, 48, 60, 71, 74, 75]. Formation control results based on nonholonomic kinematic models can be found in [6, 21, 24, 43, 52, 54, 67]. Designs for nonholonomic dynamic models appeared in [17, 27, 28, 31, 49, 79].

Among the above nonholonomic-based results, the only ones to address the formation maneuvering problem are [21, 31, 43, 67]. In [21], the problem of controlling formations was decomposed into either tracking the position and orientation of a robot relative to a lead robot or the position relative to two lead robots. A single lead robot was responsible for planning and generating the desired maneuver for the formation, which was then transmitted to the followers through a communication graph with a tree structure. In [31], a scheme that combines artificial potential functions and sliding mode control was proposed to allow the formation to track a maneuvering target. The control scheme can compensate for uncertain dynamics and is based on measurements of all agents' global position. In [43, 67], kinematic controllers were designed based on two types of position errors [71]—individual tracking errors (relative to the desired trajectory of each agent) and coordination errors for agent pairs—where the latter serves the purpose of coupling the motion of the individual agents in the formation. The control laws in [43, 67] guarantee simultaneous formation acquisition and trajectory tracking, but require measurements of all agents' global position.

The intent of our first result is to further explore the formation maneuvering control framework introduced in [43, 67] and, in particular, the interplay between the tracking and coordination errors. Specifically, we seek the following improvements to [43, 67]: a) simplify the coordination scheme to require a minimal number of control links and global position measurements, and b) extend the coordination scheme to the dynamics problem while compensating for parametric uncertainty. To this end, we consider formations of unicycle-type nonholonomic robotic vehicles with dynamics. Our solution will involve a leader-follower type coordination scheme, composed of a primary leader, secondary leaders, and a follower, where the inter-vehicle interactions are modeled by a chain-like spanning tree graph. As a result, only the global position of the primary leader is required in addition to the relative positions of the robots connected in the graph. Based on a composite Lyapunov analysis of the primary leader's tracking error and all coordination errors, we construct

a nonlinear control law that ensures all the errors are uniformly ultimately bounded. This is accomplished by exploiting the pentadiagonal structure of a matrix in the Lyapunov analysis which arises from the specific topology of our graph. For ease of explanation, the proposed control law is first developed for the nonholonomic kinematic model, and then extended to account for the vehicle dynamics using the backstepping technique [46]. In this extension, we assume the parameters in the dynamic equations are unknown, and design an adaptive controller to account for this uncertainty. Despite similarities in the open-loop error dynamics, our results in Section 3.2 differs from [43, 67] in a few aspects: i) we use a spanning tree for the coordination graph; ii) we employ a different Lyapunov function candidate and, as a result, a different control law; and iii) the stability analysis is simpler since we are only concerned with the negative definiteness of the Lyapunov function derivative in the least squares sense. With respect to [31], our control algorithm has the advantage of only depending on one robot's global position. In comparison to [21], which also uses a leader-follower strategy modeled as a tree graph, our control is not limited to the kinematics problem. A portion of the work presented in Chapter 3 appeared in [39].

Flocking and target interception controllers were introduced in [11, 9] for the single- and double-integrator models, respectively, using the distance-based, rigid graph approach from [45]. A 2D formation maneuvering controller was proposed in [5] for the double-integrator model where the group leader, who has inertial frame information, passes the information to other agents through a directed path in the graph. A limitation of this control is that it becomes unbounded if the desired formation maneuvering velocity is zero. A consensus scheme was presented in [34] using both the single- and double-integrator models where the formation translation velocity is constant and known to only two leader agents. In [66], the translational maneuvering strategy involved a leader with a constant velocity command and followers who track the leader while maintaining the formation shape. The control law, which was based on the single-integrator model, consisted of the standard gradient descent formation acquisition term plus an integral term to ensure zero-steady error with respect to the velocity command. In [72], for agents modeled by double integrators, a flocking controller was designed that allows all agents to both achieve the same velocity and reach

a desired formation in finite time. A similar problem was addressed in [20] but with asymptotic formation acquisition and velocity consensus. Recently in [50], a controller was proposed using the single-integrator model that can steer the entire formation in rotation and/or translation in 3D. The rotation component was specified relative to a body-fixed frame whose origin is at the centroid of the desired formation and needs to be known.

Various multi-agent tracking and flocking results have appeared in the literature. In [15], a control algorithm was proposed to force a multi-agent system modeled by the Euler-Lagrange equation to move inside a desired region while maintaining a predefined distance among the robots. The stability of cooperative tracking control laws for multiple robot manipulators was studied in [19] using nonlinear contraction analysis. The authors in [35] proposed a control law for the coordinated tracking problem with the presence of an observer to estimate the unknown velocities; however, their algorithm requires knowledge of a leader agent acceleration. The flocking behavior of multiple vehicles with a dynamic leader whose acceleration is known to all agents was discussed in [68],. A swarm tracking scheme via a variable structure control approach and artificial potential fields was proposed in [75]. In [65], the authors study distributed coordinated tracking problems on single- and double-integrator models; note that the observer designed in the aforementioned reference does not require leader's velocity or acceleration measurement.

In formation control, a key aspect is whether the controlled variables are the relative position vector of the agents or the inter-agent distances (i.e., norm of the relative position). The latter approach has the advantage that relative position measurements can be done in an arbitrary coordinate frame, whereas the former requires the measurements in a global coordinate frame [70]. Rigid graph theory is a natural tool for describing the multi-agent formation shape for the distance-based approach since it naturally ensures that the inter-agent distance constraints of the desired formation are enforced through the graph rigidity. The distance-based control framework has been mostly applied to the single- and double-integrator models. To the best of our knowledge, the only exception are the results in [23, 77] which considered the nonholonomic kinematic model in the design of a formation acquisition controller.

In our second result, we apply the distance-based approach to the flocking of nonholonomic kinematic agents. We assume that the desired flocking velocity is known to all agents in the formation. Similar to [23], we use a simple input transformation to convert the nonholonomic multi-agent system into the single-integrator system. As a result, we can apply the flocking controller from [11] to ensure that the desired formation is acquired and maneuvers according to the given flocking velocity. In comparison to [23], our input transformation is slightly different but more importantly, we rigorously show how it achieves the conversion to the single-integrator system using an interconnected system analysis.

We conclude the dissertation by revisiting the distance-based flocking problem but with the restriction that only a subset of the agents know the desired flocking velocity. This restriction is overcome via the design of a distributed, consensus-like observer that estimates this velocity. The premise behind the observer is that agents that do not have direct access to the flocking velocity can acquire this information from its neighbors since the graph modeling the communication and control network is connected. Distributed observers are again used to estimate these quantities based on the connectedness of the formation graph.

1.3 Dissertation Outline

This dissertation is organized as follows. In Section 1.4 below, we review some concepts of graph theory and nonlinear systems theory that will be used by the formation control algorithms. The equations of motion for the nonholonomic agents are introduced in Chapter 2. In Chapter 3, the control law for the formation maneuvering problem is first introduced at the kinematic level (Section 3.2) and then extended to the uncertain dynamics case (Section 3.3). Evaluations of the proposed control design are provided in Section 3.4 in the form of experimental results for the kinematic controller and MATLAB-based simulation results for the adaptive dynamic controllers. Chapter 4 discusses the flocking control with known desired velocity, including the control law design, closed-loop stability analysis, and experimental results. Chapter 5 presents the flocking controller with limited velocity information (Section 5.2). Experimental validations of the control solution is given in Section 5.3. The dissertation concludes with a summary of the results in

Chapter 6.

1.4 Background Material

This work utilizes some concepts of graph theory and nonlinear systems theory which are reviewed below.

An *undirected graph* G is a pair (V, E) where $V = \{1, ..., n\}$ is the set of vertices and $E \subset V \times V$ is the set of undirected edges that connect two different vertices, i.e., if vertex pair $(i, j) \in E$ then so is (j, i). We let $a \in \{1, \ldots, n(n-1)/2\}$ denote the total number of edges in E. The set of neighbors of vertex i is denoted by

$$\mathcal{N}_i(E) = \{j \in V \mid (i, j) \in E\}. \tag{1.1}$$

A graph G is said to be *complete* if every pair of distinct vertices is connected by an edge such that $a = n(n-1)/2$. A complete graph with n vertices is symbolized by K_n. A *path* is a trail that goes from an origin vertex to a destination vertex by traversing edges of the graph. An undirected graph is *connected* if there is a path between every pair of vertices of G, otherwise it is said to be disconnected. A *tree* is a connected graph in which two vertices are connected exactly by one path. Note that in a tree, cycles cannot exist. A *spanning tree* for a connected graph G is a tree containing all the vertices of G. In other words, a *spanning tree* of a graph of n vertices is a subset of $n-1$ edges that form a tree. Some general properties of spanning trees are the following [32]:

- A connected graph G can have more than one spanning tree.
- All feasible spanning trees of graph G have the same number of edges and vertices.
- Removing one edge from a spanning tree will make the graph disconnected; i.e., a spanning tree is minimally connected.
- Adding one edge to a spanning tree will create a cycle; i.e., the spanning tree is maximally acyclic.

Some of the above concepts are illustrated in Figures 1.1 and 1.2.

Let $A = [a_{ij}] \in \mathbb{R}^{n \times n}$ be the adjacency matrix defined such that $a_{ij} = 1$ if $(i, j) \in E$ and $a_{ij} = 0$

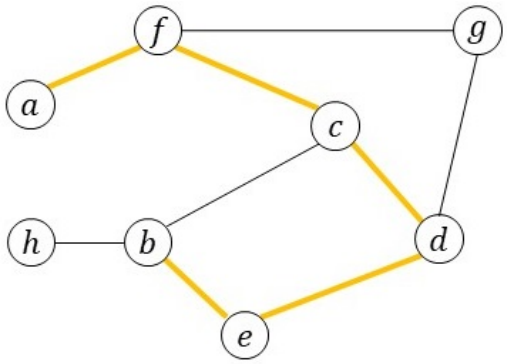

Figure 1.1. Example of a path connecting vertex a to vertex b.

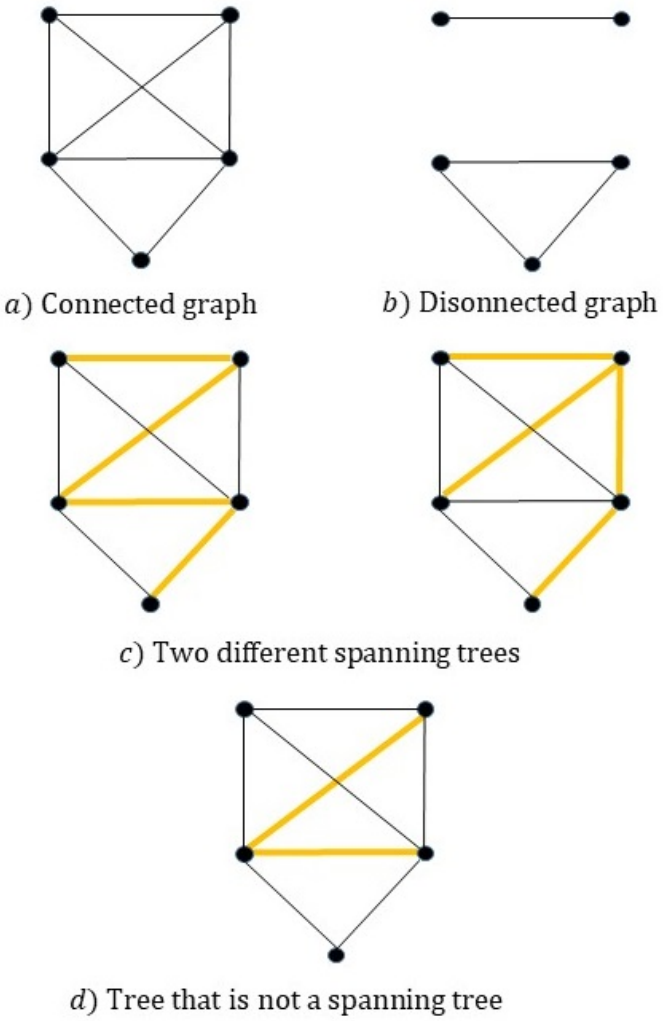

Figure 1.2. Examples of a connected graph, a tree, and spanning trees.

otherwise. Note that $a_{ij} = a_{ji}$. Let the Laplacian matrix $\mathcal{L} = [l_{ij}] \in \mathbb{R}^{n\times n}$ associated with A be defined as $l_{ii} = \sum_{j=1,j\neq i}^{n} a_{ij}$ and $l_{ij} = -a_{ij}$ for $i \neq j$. Note that $\mathcal{L}$ is symmetric positive definite and has a simple zero eigenvalue with an associated eigenvector $\mathbf{1}$ [18].

If $p_i \in \mathbb{R}^2$ is the coordinate of vertex i, then a framework F is defined as the pair (G, p) where $p = [p_1, \ldots, p_2] \in \mathbb{R}^{2n}$. In the following, we assume all frameworks have *generic* properties, i.e., the properties hold for almost all of the framework representations. This is done to exclude certain degenerate configurations such as frameworks that lie in a hyperplane (see [33] for a detailed study of generic framework).

Based on an arbitrary ordering of edges, the edge function $\phi : \mathbb{R}^{2n} \to \mathbb{R}^a$ is given by

$$\phi(p) = \left[..., \|p_i - p_j\|^2, ...\right], \quad (i,j) \in E \tag{1.2}$$

such that its kth component, $\|p_i - p_j\|^2$, relates to the kth edge of E connecting the ith and jth nodes. The rigidity matrix $R : \mathbb{R}^{2n} \to \mathbb{R}^{a\times 2n}$ is given by

$$R(p) = \frac{1}{2}\frac{\partial \phi(p)}{\partial p} \tag{1.3}$$

where $\text{rank}[R(p)] \leq 2n - 3$ [2].

An isometry of $\mathbb{R}^2$ is a bijective map $\mathcal{T} : \mathbb{R}^2 \to \mathbb{R}^2$ satisfying [36]

$$\|w - z\| = \|\mathcal{T}(w) - \mathcal{T}(z)\|, \quad \forall w, z \in \mathbb{R}^2. \tag{1.4}$$

This map includes rotations and translations of the vector $w - z$. Two frameworks are said to be *isomorphic* in $\mathbb{R}^2$ if they are related by an isometry. In this dissertation, we will represent the collection of all frameworks that are isomorphic to F by $\text{Iso}(F)$. It is important to point out that (1.2) is invariant under isomorphic motions of the framework.

Frameworks (G, p) and $(G, \hat{p})$ are equivalent if $\phi(p) = \phi(\hat{p})$, and are congruent if $\|p_i - p_j\| = \|\hat{p}_i - \hat{p}_j\|$, $\forall i, j \in V$ [37]. The necessary and sufficient condition for a generic framework (G, p)

to be infinitesimally rigid is $\text{rank}[R(p)] = 2n - 3$ [36]. An infinitesimally rigid framework is minimally rigid if and only if $a = 2n - 3$ [1]. If the infinitesimally rigid frameworks (G, p) and $(G, \hat{p})$ are equivalent but not congruent, then they are referred to as *ambiguous* [1]. The notation $\text{Amb}(F)$ will be used here to represent the collection of all frameworks that are ambiguous to the infinitesimally rigid framework F. All frameworks in $\text{Amb}(F)$ are also assumed to be infinitesimally rigid. According to [1] and Theorem 3 of [4], this assumption holds almost everywhere; therefore, it is not restrictive.

Lemma 1 *[10] Consider two frameworks $F = (G, p)$ and $\bar{F} = (G, \bar{p})$ sharing the same graph $G = (V, E)$ and the function*

$$\Lambda(\bar{F}, F) = \sum_{(i,j)\in E} \left(\|\bar{p}_i - \bar{p}_j\| - \|p_i - p_j\|\right)^2. \tag{1.5}$$

If F is infinitesimally rigid and $\Lambda(\bar{F}, F) \leq \varepsilon$ where ε is a sufficiently small positive constant, then $\bar{F}$ is also infinitesimally rigid.

Lemma 2 *[11] For any $x \in \mathbb{R}^2$, $R(p)(1_n \otimes x) = 0$ where 1_n is the $n \times 1$ vector of ones.*

The following stability theorems will prove useful.

Theorem 1 *[40] Consider the system $\dot{x} = f(x, u)$ where x is the state, u is the control input, and $f(x, u)$ is locally Lipschitz in (x, u) in some neighborhood of $(x = 0, u = 0)$. Then, the system is locally input-to-state stable if and only if the unforced system $\dot{x} = f(x, 0)$ has a locally asymptotically stable equilibrium point at the origin.*

Theorem 2 *[51] Consider the interconnected system*

$$\begin{aligned} \Sigma_1\text{:} \quad & \dot{x} = f(x, y) \\ \Sigma_2\text{:} \quad & \dot{y} = g(y). \end{aligned} \tag{1.6}$$

if subsystem Σ_1 with input y is locally input-to-state stable and $y = 0$ is a locally stable equilibrium point of subsystem Σ_2, then $[x, y] = 0$ is a locally asymptotically stable equilibrium point of the interconnected system.

Finally, the following metric will be used to denote the "distance" between a point and a set:

$$\operatorname{dist}(\zeta, \mathcal{M}) = \inf_{x \in \mathcal{M}} \|\zeta - x\| \tag{1.7}$$

for points $\zeta, x \in \mathbb{R}^2$ and a set $\mathcal{M}$.

Chapter 2. System Model

In this chapter, we introduce the equations of motion for the multi-agent system. We consider a system of n wheeled nonholonomic robots moving autonomously on the plane. We assume the wheels operate under the conditions of pure rolling and no slipping. This condition is known as a *nonholonomic constraint*, and is the main feature of the kinematic model of wheeled mobile robots.

To explain this feature, consider a single wheel (a.k.a. unicycle) moving on the plane as shown in Figure 2.1, where $q = [x, y, \theta]$ denotes the wheel pose. Under the rolling without slipping condition, the wheel is not able to move sideways. Thus, the linear velocity of the wheel center has no lateral component and lies in the body plane of the wheel. In other words, the wheel's velocity cannot take independent values, and must satisfy the following constraint [22]

$$w^\intercal \dot{q} = 0 \tag{2.1}$$

where $w = [\sin\theta, -\cos\theta, 0]$. The constraint equation (2.1) is a common example of a *Pfaffian* constraint, which has the general form [22]

$$A(q)\dot{q} = 0 \tag{2.2}$$

where $A : \mathbb{R}^n \to \mathbb{R}^{k\times n}$ and $k < n$. Note that Pfaffian constraints are *linear* in the velocities. If

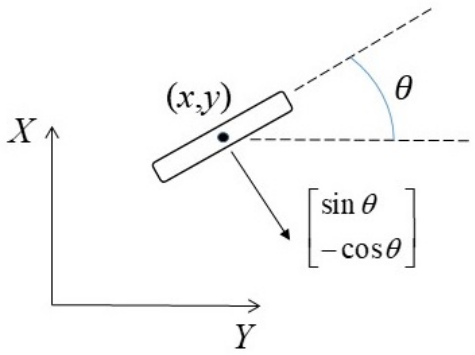

Figure 2.1. Unicycle kinematics.

(2.2) can be integrated to yield

$$h(q) = c \tag{2.3}$$

where $h : \mathbb{R}^n \to \mathbb{R}^k$ such that $\partial h/\partial q = A(q)$ and $c \in \mathbb{R}^k$ contains the integration constants, then the Pfaffian constraint is said to be holonomic (a pure geometric constraint). Otherwise, (2.2) is called nonholonomic (a kinematic constraint).

From (2.2), we know that all possible velocities are contained in the null space of the matrix $A(q)$. Since in our case, $A(q) = w^\intercal$, we have that

$$\text{Null}(A(q)) = \text{span}\left\{ \begin{bmatrix} \cos\theta \\ \sin\theta \\ 0 \end{bmatrix}, \begin{bmatrix} 0 \\ 0 \\ 1 \end{bmatrix} \right\}, \tag{2.4}$$

and therefore,

$$\dot{q} = \begin{bmatrix} \cos\theta \\ \sin\theta \\ 0 \end{bmatrix} v + \begin{bmatrix} 0 \\ 0 \\ 1 \end{bmatrix} \omega \tag{2.5}$$

where v is the linear velocity in the direction of θ and ω is the steering velocity about the vertical axis. Equation (2.5) is called the *kinematic model* of the unicycle.

Now, we turn our attention to the multi-agent system model. Consider the ith robot depicted in Figure 2.2, where $\{X_0, Y_0\}$ is a reference frame fixed to the Earth and $\{X_i, Y_i\}$ is the moving reference frame attached to the robot such that the X_i-axis is aligned with robot's heading direction, which is denoted by the angle θ_i and measured counterclockwise from the X_0-axis. It is assumed that the robot's center of mass is coincident with its center of rotation located at point C_i. We consider that each robot is a unicycle vehicle governed by following equations of motion [25]

$$\dot{q}_i = S(\theta_i)\eta_i \tag{2.6}$$

$$M_i\dot{\eta}_i + D_i\eta_i = u_i \tag{2.7}$$

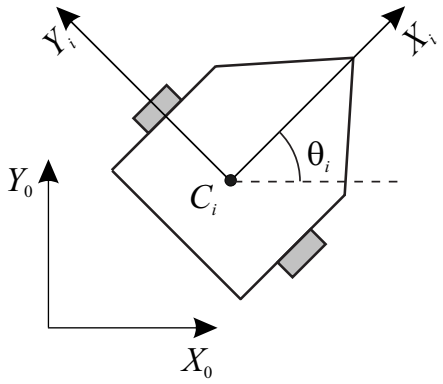

Figure 2.2. Schematic of the unicycle vehicle.

for $i = 1, 2, ..., n$. The robot kinematics is given by (2.6), where $q_i = [x_i, y_i, \theta_i]$ denotes the position and orientation of $\{X_i, Y_i\}$ relative to $\{X_0, Y_0\}$, $\eta_i = [v_i, \omega_i]$, v_i is the robot's linear velocity in the direction of θ_i, ω_i is the robot's steering velocity about the vertical axis passing through C_i, and

$$S(\theta_i) = \begin{bmatrix} \cos\theta_i & 0 \\ \sin\theta_i & 0 \\ 0 & 1 \end{bmatrix}. \tag{2.8}$$

Note that (2.6) and (2.8) are equivalent to (2.5). The robot dynamics is described by (2.7), where $M_i = \text{diag}(m_i, J_i)$, m_i and J_i are the vehicle mass and mass moment of inertia about the vertical axis, respectively, $D_i \in \mathbb{R}^{2\times 2}$ is the constant damping matrix, and $u_i \in \mathbb{R}^2$ represents the force/torque-level control input provided by the drive train actuators.

Chapter 3. Formation Maneuvering Control

In this chapter, we present a leader-follower type solution to the formation maneuvering problem for multiple, nonholonomic wheeled mobile robots. Our solution is based on the graph that models the coordination among the robots being a spanning tree. Our control law ensures, in the least squares sense, that the robots globally asymptotically acquire a given planar formation while the formation as a whole globally asymptotically tracks a desired trajectory. The control law is first designed at the kinematic level and then extended to the dynamic level. In the latter, we consider that parametric uncertainty exists in the equations of motion. These uncertainties are accounted for using an adaptive control scheme. The proposed formation maneuvering controls are demonstrated by experimental and numerical simulations of five vehicles.

3.1 Problem Statement

Our control objective is to ensure that the system of n nonholonomic robots acquires a specified two-dimensional formation and maneuvers cohesively according to a predefined desired trajectory.

The information exchange between robots is modeled by graph $T(V, E)$, which should be a spanning tree of the complete graph K_n.[1] The spanning tree guarantees that the least number of control links (edges) between the robots in the graph is used to meet the control objective. The spanning tree is also motivated by our proposed collaboration protocol for the robots, which includes three categories of agents. In particular, we will designate one robot as the *primary leader*, which for notational convenience will be robot 1, who knows its global position (i.e., with respect to $\{X_0, Y_0\}$). The *secondary leaders* are robots who have a dual roles: they follow the primary leader or a secondary leader, but also serve as a leader for other robots. Finally, the *follower* is the robot that simply follows a secondary leader with no leadership role. Secondary leaders and followers can only measure their *relative* position to other robots to which they are connected in T.

Our control approach will require that graph T have a chain-like form: vertex 1 (primary leader) is only connected to vertex 2, vertex i for $i = 2, \ldots, n-1$ (secondary leaders) is only

[1] This requirement is simply for the purpose of maximizing the number of choices for the spanning tree.

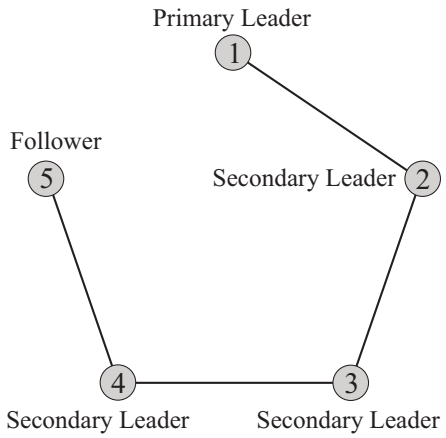

Figure 3.1. Spanning tree example with five robots.

connected to vertices $i-1$ and $i+1$, and vertex n (follower) is only connected to vertex $n-1$. Figure 3.1 shows an example of a required spanning tree T for the case of five robots.

We will quantify the control objective by defining two types of position errors. The first one is the standard *tracking* error for each individual robot:

$$e_i = q_{di} - q_i, \quad i \in V \tag{3.1}$$

where $q_{di}(t) \in \mathbb{R}^3$ denotes the desired trajectory for robot i (below we describe how q_{di} is generated) dictated by the desired formation shape and maneuver. We also introduce the following *coordination* error between robots i and j [43, 67, 71]

$$\varepsilon_{ij} = e_i - e_j, \quad (i,j) \in E \tag{3.2}$$

where E is edge set of the spanning tree. The coordination errors will couple the motion of robots so that the desired formation maneuvering is accomplished by only measuring q_1 and $q_i - q_j$, $(i,j) \in E$. That is, from (3.1) and (3.2), we have that

$$\varepsilon_{ij} = q_{di} - q_{dj} - (q_i - q_j)\,, \tag{3.3}$$

which is only dependent on the relative position of robots i and j. Our problem statement is then to design $u_i = u_i(t, \theta_i, \eta_i, q_1, q_i - q_j)$, $\forall i \in V$ and $\forall (i,j) \in E$ in (2.7) such that

$$\lim_{t \to \infty} \left(|e_i(t)|, |\varepsilon_{ij}(t)| \right) \leq \delta \tag{3.4}$$

for $\forall i \in V$ and $\forall (i,j) \in E$, where δ is an arbitrarily small constant.

The desired trajectory of each robot needs to satisfy the nonholonomic constraint of the unicycle vehicle given by (2.6). That is,

$$\dot{q}_{di} = S\left(\theta_{di}\right) \eta_{di} \tag{3.5}$$

where $q_{di} = (x_{di}, y_{di}, \theta_{di})$, and $\eta_{di} = (v_{di}, \omega_{di})$ includes the desired translational and rotational speeds such that $v_{di}(t) \neq 0$, $\forall t$. This condition on v_{di} stems from the potential singularity in the relationship $\omega_{di} = \left(\dot{x}_{di}\ddot{y}_{di} - \ddot{x}_{di}\dot{y}_{di}\right)/v_{di}^2$, which can be derived from (3.5) and its derivative. However this singularity can be diminished by using a different control point on the vehicle other than on the axis of the two wheels. We assume the desired trajectory is generated such that $q_{di}(t)$, $\dot{q}_{di}(t)$, $\eta_{di}(t)$, and $\dot{\eta}_{di}(t)$, $i = 1, \ldots, n$ are bounded for all time. The signal $q_{di}(t)$ is usually known in advance and therefore can be stored on the ith robot's microcontroller.

Remark 1 *Different approaches can be used to acquire the linear position signals needed by the control. The most direct approach is to equip each robot with a GPS and then have the signals broadcast between the robots using a local wireless network. This approach has the disadvantage of reduced accuracy when the line of sight between the GPS receiver and satellite is obstructed (e.g., indoor operation, urban areas, dense vegetation, underwater). An alternative approach for GPS-denied environments is to use a suite of onboard sensors. Specifically, one can measure the relative linear positions in (3.3) using, for example, a rangefinder, camera, and compass, and measure the global position of the primary leader using an inertial navigation system coupled to a Kalman filter. Finally, the robots' heading angles can be measured with a compass, while velocity signals can be determined by numerically differentiating and low-pass filtering the position signals.*

Remark 2 *In theory, a formation control law could be designed just based on (3.1) such that each*

robot tracks its own desired trajectory, independently of one another. This however has the disadvantage that a) perturbations from the desired trajectory will distort the formation shape without a mechanism for self-correction, and b) the control will depend on the global position of all robots. These problems are avoided by introducing (3.2) in the control scheme along with the chain-like topology for the graph .

3.2 Kinematic Control

We first consider the kinematic control problem by treating η_i in (2.6) as the control input. To this end, we begin by expressing the tracking error (3.1) with respect to the moving reference frame $\{X_i, Y_i\}$ as follows [25, 38]

$$s_i = R^\intercal(\theta_i) e_i \tag{3.6}$$

where $R(\theta_i)$ is the rotation matrix defined as

$$R(\theta_i) = \begin{bmatrix} \cos\theta_i & -\sin\theta_i & 0 \\ \sin\theta_i & \cos\theta_i & 0 \\ 0 & 0 & 1 \end{bmatrix}. \tag{3.7}$$

Differentiating (3.6) with respect to time yields

$$\begin{aligned} \dot{s}_i &= \dot{R}^\intercal(\theta_i) e_i + R^\intercal(\theta_i)\left(\dot{q}_{di} - \dot{q}_i\right) \\ &= \omega_i Q s_i + R^\intercal(\theta_i) S(\theta_{di}) \eta_{di} - P\eta_i \end{aligned} \tag{3.8}$$

where

$$Q = \begin{bmatrix} 0 & 1 & 0 \\ -1 & 0 & 0 \\ 0 & 0 & 0 \end{bmatrix}, \quad P = \begin{bmatrix} 1 & 0 \\ 0 & 0 \\ 0 & 1 \end{bmatrix}, \tag{3.9}$$

$\dot{R}^\intercal(\theta_i) = \omega_i Q R^\intercal(\theta_i)$, and $S(\cdot)$ was defined in (2.8).

Now, consider the Lyapunov function candidate

$$V(z) = \frac{1}{2} s_1^T s_1 + \frac{1}{2} \sum_{(i,j)\in E} \varepsilon_{ij}^\intercal \varepsilon_{ij} = \frac{1}{2} z^\intercal z \tag{3.10}$$

where

$$z = (s_1, \ldots, \varepsilon_{ij}, \ldots) \in \mathbb{R}^{3n}, \quad \forall (i,j) \in E. \tag{3.11}$$

It is important to note that (3.11) is a function of all coordination errors but only the primary leader's tracking error.

The time derivative of (3.10) is given by

$$\begin{aligned} \dot{V} = \; & s_1^\intercal \left[R^\intercal(\theta_1) S(\theta_{d1}) \eta_{d1} - P\eta_1 \right] + \sum_{(i,j)\in E} \varepsilon_{ij}^\intercal \left[S(\theta_{di})\eta_{di} \right. \\ & \left. - S(\theta_i)\eta_i - S(\theta_{dj})\eta_{dj} + S(\theta_j)\eta_j \right] \end{aligned} \tag{3.12}$$

where we used the fact that Q is skew-symmetric. After some manipulations, we can rewrite (3.12) in the following form

$$\dot{V} = z^\intercal \left[K(\theta)\, \eta + H(\theta_1, t) \right] \tag{3.13}$$

where $\eta = (\eta_1, \ldots, \eta_n) \in \mathbb{R}^{2n}$, $\theta = (\theta_1, \ldots, \theta_n) \in \mathbb{R}^n$, and $K \in \mathbb{R}^{3n \times 2n}$ and $H \in \mathbb{R}^{3n}$ are defined as

$$K(\theta) = \begin{bmatrix} -P & 0_{3\times 2} & 0_{3\times 2} & 0_{3\times 2} & \cdots & 0_{3\times 2} \\ -S(\theta_1) & S(\theta_2) & 0_{3\times 2} & 0_{3\times 2} & \cdots & 0_{3\times 2} \\ 0_{3\times 2} & -S(\theta_2) & S(\theta_3) & 0_{3\times 2} & \cdots & 0_{3\times 2} \\ 0_{3\times 2} & 0_{3\times 2} & -S(\theta_3) & S(\theta_4) & 0_{3\times 2} & 0_{3\times 2} \\ \ddots & \ddots & \ddots & \ddots & \ddots & \ddots \\ 0_{3\times 2} & 0_{3\times 2} & \cdots & 0_{3\times 2} & -S(\theta_{n-1}) & S(\theta_n) \end{bmatrix} \tag{3.14}$$

$$H(\theta_1, t) = \begin{bmatrix} R^\intercal(\theta_1) S(\theta_{d1}) \eta_{d1} \\ S(\theta_{d1}) \eta_{d1} - S(\theta_{d2}) \eta_{d2} \\ \vdots \\ S(\theta_{d(n-1)}) \eta_{d(n-1)} - S(\theta_{dn}) \eta_{dn} \end{bmatrix}. \tag{3.15}$$

Remark 3 *The structure of matrix $K(\theta)$ in (3.14) stems from the chain-like form of graph T, and is crucial for the proposed control design and its stability analysis. In particular, it can be proven that (3.14) has full column rank (see Appendix A).*

In the following theorem, we give a solution to the kinematic control problem that is valid in the *least squares sense*.

Theorem 3 The kinematic control

$$\eta = -K^\dagger(\theta) \left[\lambda_1 z + H(\theta_1, t) \right], \tag{3.16}$$

where λ_1 is a $3n \times 3n$ diagonal, positive-definite, control gain matrix and $K^\dagger$ is the *pseudo-inverse* of (3.14) defined as

$$K^\dagger = (K^\intercal K)^{-1} K^\intercal, \tag{3.17}$$

ensures that (3.4) is met with global exponential decay and that all other system signals are globally bounded.

Proof. If we can specify η to satisfy

$$K\eta + H = -\lambda_1 z, \tag{3.18}$$

then we know from (3.13) that

$$\dot{V} = -z^\intercal \lambda_1 z. \tag{3.19}$$

Along with the form of (3.10), this would indicate that $z = 0$ is exponentially stable [40].

Notice that K in (3.14) does not have full row rank since the system (3.18) is overdetermined. Therefore, the exact solution

$$\eta^* = -K^\intercal (KK^\intercal)^{-1}(\lambda_1 z + H) \tag{3.20}$$

cannot be used. However, the fact that K has full column rank means the matrix $K^\intercal K$ is invertible. Therefore, we seek a solution for (3.18) that minimizes the energy of the error [47]

$$J(\eta) = \|K\eta^* - K\eta\|^2 = \|(-\lambda_1 z - H) - K\eta\|^2 \tag{3.21}$$

where $\|\cdot\|$ denotes the Euclidean norm. This solution, which is called the *least squares solution*, is given by (3.16). Since this is an approximate solution for (3.18), this equation becomes

$$K\eta + H = -\lambda_1 z + r \tag{3.22}$$

where r is the least squares residual. Since matrix K has full column rank, the solution (3.16) is unique and r can be upper bounded as follows [59]

$$\|r\| \leq \sqrt{a_1 + a_2 \|\eta\|^2} \tag{3.23}$$

where a_1 and a_2 are some positive constants. From (3.16), it is not difficult to see that

$$\|\eta\| \leq b_1 + b_2 \|z\| \tag{3.24}$$

where b_1 and b_2 are some positive constants. Therefore, substituting (3.24) into (3.23) yields

$$\|r\| \leq \sqrt{c_1 + c_2 \|\eta\| + c_3 \|\eta\|^2} \leq c_4 + c_5 \|z\| \tag{3.25}$$

where the c_i's are some positive constants.

Now, if we substitute (3.22) in (3.13), we obtain

$$\dot{V} = -z^{\intercal}\lambda_1 z + z^{\intercal} r. \tag{3.26}$$

By using (3.25) and letting $\lambda_1 = \lambda_1^{'} + \lambda_1^{''}$, we can upper bound (3.26) as follows

$$\begin{aligned} \dot{V} &\leq -z^{\intercal}\lambda_1 z + \|z\| \left(c_4 + c_5 \|z\|\right) \\ &\leq -(\sigma_{\min}(\lambda_1^{'}) - c_5) \|z\|^2 + c_4 \|z\| - \sigma_{\min}(\lambda_1^{''}) \|z\|^2 \\ &\leq -(\sigma_{\min}(\lambda_1) - c_5) \|z\|^2 + \frac{c_4^2}{4\sigma_{\min}(\lambda_1^{''})} \end{aligned} \tag{3.27}$$

where $\sigma_{\min}(\cdot)$ represents the minimum eigenvalue. If $\sigma_{\min}(\lambda_1) > c_5$ and $\epsilon := c_4^2 / \left[4\sigma_{\min}(\lambda_1^{''})\right]$, we have from (3.10) and (3.27) that

$$\dot{V} \leq -\beta \|z\|^2 + \epsilon \leq -2\beta V + \epsilon, \tag{3.28}$$

where $\beta := \sigma_{\min}(\lambda_1) - c_5 > 0$, which indicates that $z(t)$ is globally uniformly ultimately bounded [63]. This means that

$$\lim_{t\to\infty} \|z(t)\| \leq \sqrt{\frac{\epsilon}{2\beta}} := \delta \tag{3.29}$$

where the steady-state error can be made arbitrarily small by increasing $\sigma_{\min}(\lambda_1)$.

From (3.28), (3.29), and the definition of z, we know that $\lim_{t\to\infty} \left(|s_1(t)|, |\varepsilon_{ij}(t)|\right) \leq \delta$, $(i,j) \in E$ with an exponential convergence rate controlled by $\sigma_{\min}(\lambda_1)$. From (3.6), we then know that $\lim_{t\to\infty} |e_1(t)| \leq \delta$ globally exponentially fast. Given the spanning tree nature of the graph, we can recursively use (3.2) starting from the primary leader to show that $\lim_{t\to\infty} |e_i(t)| \leq \delta$, $i = 2, \ldots, n$ globally exponentially fast.

Based on (3.1) and the assumption that $q_{di}(t)$, $i = 1, \ldots, n$ is bounded, we know that $q_i(t)$, $i = 1, \ldots, n$ is bounded for all time. Since $e_i(t)$, $i = 1, \ldots, n$ is bounded, we know from (3.6) that $s_i(t)$, $i = 2, \ldots, n$ is bounded. From (3.14) and (3.15), we have that $K(\theta)$ and $H(\theta_1, t)$ are

bounded. Thus, we know from (3.16) that $\eta(t)$ is bounded. From (2.6) and (2.8), we can conclude that $\dot{q}_i(t)$, $i = 1, \ldots, n$ is bounded. ■

3.3 Adaptive Dynamics Control

The kinematic controller assumes the control inputs are the translational and angular speeds of the vehicle. However, these are *states* of the dynamic system with the actual control inputs being the torque/force produced by the drivetrain motors. In this section, we extend the kinematic control law to account for the robot dynamics (2.7) so we can design actuator-level control inputs. We will assume that uncertainties exist in the parameters of (2.7), which will be accounted for by the design of an adaptive control law. To this end, we exploit the fact that (2.7) is linear in the unknown parameters:

$$M_i\mu + D_i\eta_i = Y_i(\mu, \eta_i)\phi_i, \quad \forall \mu = (\mu_1, \mu_2) \tag{3.30}$$

where

$$Y_i = \begin{bmatrix} \mu_1 & 0 & v_i & \omega_i & 0 & 0 \\ 0 & \mu_2 & 0 & 0 & v_i & \omega_i \end{bmatrix} \tag{3.31}$$

is the 2×6 regression matrix,

$$\phi_i = (m_i, J_i, [D_i]_{11}, [D_i]_{12}, [D_i]_{21}, [D_i]_{22}) \tag{3.32}$$

is the *unknown*, constant parameter vector, and $[\cdot]_{ij}$ denotes the ijth element of the matrix. We assume each parameter in (3.32) lies in a known compact set. That is, parameter $\bullet \in [\bullet_{\min}, \bullet_{\max}]$ where $\bullet_{\min}$ and $\bullet_{\max}$ are known constants. Let the stack vector of all parameters for all robots be $\Phi = \{\Phi_i\} := (\phi_1, ..., \phi_n) \in \mathbb{R}^{6n}$ such that $\Phi_1 = m_1$, $\Phi_2 = J_1$, $\ldots$, $\Phi_7 = m_2$, etc., where $\Phi \in \Omega := \{\Phi : \|\Phi\| \leq \varrho\}$ and ϱ is a known constant dependent on the compact sets of the individual parameters Φ_i.

The formation controller will include a dynamic estimate of (3.32), whose adaptation law will be part of the control design. To this end, let $\hat{\Phi}(t) \in \mathbb{R}^{6n}$ be the parameter estimate vector, and

define the corresponding parameter estimation error as

$$\tilde{\Phi} = \hat{\Phi} - \Phi. \tag{3.33}$$

We also introduce the new error variable

$$\rho = \eta - \eta_f, \tag{3.34}$$

where $\eta_f \in \mathbb{R}^{2n}$ denotes the *fictitious* velocity input, to facilitate the use of the backstepping technique [46]. Finally, we introduce the new Lyapunov function candidate

$$V_a = V(z) + \frac{1}{2}\rho^\intercal M \rho + \frac{1}{2}\tilde{\Phi}^\intercal \Gamma^{-1} \tilde{\Phi} \tag{3.35}$$

where V was defined in (3.10), $M = \text{diag}(M_1, ..., M_n)$, and $\Gamma \in \mathbb{R}^{6n \times 6n}$ is a diagonal, positive definite, adaptation gain matrix.

In order to solve the adaptive dynamics control problem, we propose the following adaptive control

$$\begin{aligned} u &= -\lambda_2 \rho - K^\intercal(\theta) z + Y(\dot{\eta}_f, \eta)\hat{\Phi} && (3.36)\\ \eta_f &= -K^\dagger(\theta)\left[\lambda_1 z + H(\theta_1, t)\right] && (3.37)\\ \dot{\hat{\Phi}} &= -\Gamma \text{Proj}(\pi, \hat{\Phi}), && (3.38)\\ \pi &= Y^\intercal(\dot{\eta}_f, \eta)\rho && (3.39) \end{aligned}$$

where $u = (u_1, ..., u_n) \in \mathbb{R}^{2n}$, λ_1 is a $3n \times 3n$ diagonal, positive-definite, control gain matrix, λ_2 is a $2n \times 2n$ diagonal, positive-definite, control gain matrix, and $\text{Proj}(\pi, \hat{\Phi})$ is the projection operator

given by [8]

$$\text{Proj}(\pi, \hat{\Phi}) = \pi - \frac{\left(\frac{p(\hat{\Phi}) + \left|p(\hat{\Phi})\right|}{2}\right)\left(\frac{\nabla p(\hat{\Phi})^\intercal \pi + \left|\nabla p(\hat{\Phi})^\intercal \pi\right|}{2}\right)\nabla p(\hat{\Phi})}{\nabla p(\hat{\Phi})^\intercal \nabla p(\hat{\Phi})} \tag{3.40}$$

with

$$p(\hat{\Phi}) = \frac{\hat{\Phi}^\intercal \hat{\Phi} - \varrho^2}{c^2 + 2c\varrho}, \tag{3.41}$$

c an arbitrary positive constant, and ∇ the gradient operator. If $\hat{\Phi}(0) \in \Omega$, the above projection operator is known to have the following properties [8]:

P1. $\left\|\hat{\Phi}(t)\right\| \leq \varrho + c \ \forall t \geq 0$;

P2. $\tilde{\Phi}^\intercal \text{Proj}(\pi, \hat{\Phi}) \geq \tilde{\Phi}^\intercal \pi$.

The following theorem depicts the main result of this section.

Theorem 4 The adaptive control in (3.36)-(3.39) ensures that (3.4) is satisfied with global exponential decay and that all other system signals are globally bounded.

Proof. First, note from (3.35) that[2]

$$\begin{aligned} V_a &\leq \frac{1}{2}\|z\|^2 + \frac{\sigma_{\max}(M)}{2}\|\rho\|^2 + \frac{\sigma_{\max}(\Gamma^{-1})}{2}\left\|\tilde{\Phi}\right\|^2 \\ &\leq \frac{1}{2}\max\{1, \sigma_{\max}(M)\}\left(\|z\|^2 + \|\rho\|^2\right) + \frac{\sigma_{\max}(\Gamma^{-1})}{2}\left(\left\|\hat{\Phi}\right\| + \|\Phi\|\right)^2 \\ &\leq \frac{1}{2}\max\{1, \sigma_{\max}(M)\}\left(\|z\|^2 + \|\rho\|^2\right) + \frac{\sigma_{\max}(\Gamma^{-1})}{2}(2\varrho + c)^2 \\ &= \zeta_1\left(\|z\|^2 + \|\rho\|^2\right) + \zeta_2 \end{aligned} \tag{3.42}$$

where $\sigma_{\max}(\cdot)$ denotes maximum eigenvalue,

$$\zeta_1 := \frac{1}{2}\max\{1, \sigma_{\max}(M)\}, \quad \text{and} \quad \zeta_2 := \frac{\sigma_{\max}(\Gamma^{-1})}{2}(2\varrho + c)^2.$$

[2]The purpose of using the projection algorithm on the adaptation law is to ensure that V_a can be upper bounded as in (3.42).

After taking the time derivative of (3.35), we obtain

$$\begin{aligned}\dot{V}_a &= z^\intercal \left[K\left(\theta\right)\eta + H(\theta_1, t)\right] + \rho^\intercal \left(u - D\eta - M\dot{\eta}_f\right) + \tilde{\Phi}^\intercal \Gamma^{-1}\dot{\hat{\Phi}} \\ &= z^\intercal \left[K\left(\theta\right)\eta_f + H(\theta_1, t)\right] + \rho^\intercal \left[u - Y(\dot{\eta}_f, \eta)\phi + K^\intercal(\theta) z\right] + \tilde{\Phi}^\intercal \Gamma^{-1}\dot{\hat{\Phi}} \end{aligned} \tag{3.43}$$

where (2.7), (3.13), (3.30), and (3.34) were used, $D = \text{diag}(D_1, ..., D_n)$, and $Y(\dot{\eta}_f, \eta) = \text{diag}(Y_1(\dot{\eta}_{f_1}, \eta_1)$, $..., Y_n(\dot{\eta}_{f_n}, \eta_n))$. Now, substituting (3.36)-(3.39) and (3.22) with η replaced by η_f into (3.43) yields

$$\dot{V}_a = -z^\intercal \left(\lambda_1 z + r\right) - \rho^\intercal \lambda_2 \rho + \tilde{\Phi}^\intercal \left(Y^\intercal(\dot{\eta}_f, \eta)\rho - \text{Proj}(\pi, \hat{\Phi})\right). \tag{3.44}$$

Upon use of (3.27) and property P2 of the projection, we obtain

$$\dot{V}_a \leq -\min\{\beta, \sigma_{\min}(\lambda_2)\} \left(\|z\|^2 + \|\rho\|^2\right) + \epsilon. \tag{3.45}$$

Finally, applying (3.42) and (3.35) to (3.45) yields

$$\dot{V}_a \leq -\frac{\min\{\beta, \sigma_{\min}(\lambda_2)\}}{\zeta_1} V_a + \epsilon + \frac{\zeta_2 \min\{\beta, \sigma_{\min}(\lambda_2)\}}{\zeta_1} \tag{3.46}$$

from which we can conclude that $z(t)$ and $\rho(t)$ are globally uniformly ultimately bounded. As the in proof of Theorem 1, we can show that (3.4) holds with $\delta = \sqrt{\frac{\epsilon\zeta_1}{\min\{\beta, \sigma_{\min}(\lambda_2)\}} + \zeta_2}$.

Since $q_{di}(t)$ is bounded by assumption, we know $q_i(t)$ is bounded for all time from (3.1). Again, we can follow the proof of Theorem 1 to show that $s_i(t)$ and $\eta_f(t)$ are bounded. Then, using (3.34), we have that $\eta(t)$ is bounded. From (2.6) and (2.8), we conclude that $\dot{q}_i(t)$ is bounded. As shown in Appendix B, $\dot{\eta}_f$ is a function of the variables θ, η, z, and t; hence, we know that $\dot{\eta}_f(t)$ is bounded. Due to property P1 of the projection, we know that $\hat{\Phi}(t)$ is bounded. Consequently, we can show $u(t)$ and $\dot{\hat{\Phi}}(t)$ are bounded using (3.36) and (3.38). Finally, we can use (2.7) to conclude that $\dot{\eta}_i(t)$ is bounded. ■

Remark 4 *Note that (3.37) is the right-hand side of (3.16). Also, the expression for its derivative*

$\dot{\eta}_f$, which is needed in (3.36) and (3.38), is explicitly given in Appendix B.

Remark 5 *To implement a kinematic controller in practice, one includes the kinematic control law as the desired velocity in a lower level, velocity control loop. That is, one simply sets u in (3.36) to $u = -\lambda_2 \rho$ where ρ, defined in (3.34), is the velocity error. Since this simplified actuator-level control law does not explicitly compensate for the vehicle dynamics, it cannot be proven to globally stabilize the closed-loop system, and will likely yield a worse performance than a control law that incorporates dynamic model-based feedforward terms.*

3.4 Control Evaluation

3.4.1 Kinematic Control Experiment

To demonstrate the performance of the kinematic controller from Section 3.2, we conducted an experiment on the *Robotarium* system [62], which is a swarm robotics testbed that uses the GRITSBot as the mobile robot platform [61]. The testbed arena has a 8×12 ft^2 area on which multiple robots can be deployed. The GRITSBot is a low-cost, wheeled robot equipped with a suite of onboard sensors, wireless communication, battery, and processing boards, and has a footprint of approximately 3×3 cm^2. An overhead camera and a unique identification tag atop each robot's chassis provide a position tracking system for their motion. A picture of Robotarium and the GRITSBot are shown in Figure 3.2. Robotarium is ideal for testing kinematic control laws since it uses velocity-level commands as inputs to the robots with the low-level, velocity control loop being invisible to the user. The desired formation maneuver was a regular pentagon that moves as a virtual rigid body around a circle. To this end, the desired trajectory for the geometric center of the pentagon was chosen as $q_d^{cg}(t) = (5\cos t \text{ cm}, 5\sin t \text{ cm}, t + \pi/2 \text{ rad})$. From this trajectory, we determined the corresponding trajectory for each robot to be governed by (3.5) with $\eta_{di} = (5$

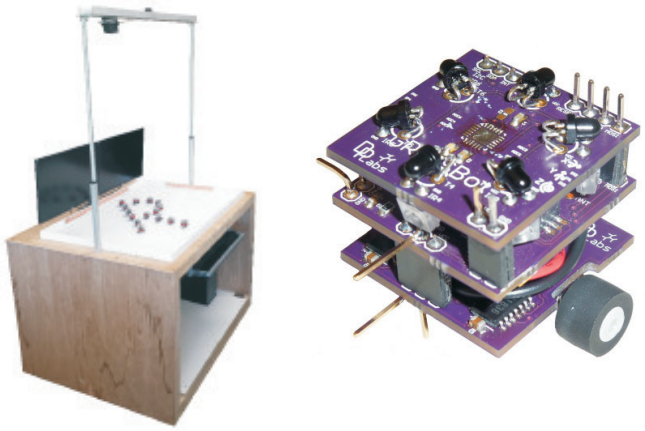

Figure 3.2. The Robotarium (left) and the GRITSBot (right)

cm/s, 1 rad/s), $i = 1, ..., n$, and initial conditions

$$\begin{aligned}
q_{d1}(0) &= (5 \text{ cm}, 10 \text{ cm}, \pi/2 \text{ rad}), \; q_{d2}(0) = (5 + 10\cos\pi/10 \text{ cm}, 10\sin\pi/10 \text{ cm}, \pi/2 \text{ rad}), \\
q_{d3}(0) &= (5 + 10\sin\pi/5 \text{ cm}, -10\cos\pi/5 \text{ cm}, \pi/2 \text{ rad}), \\
q_{d4}(0) &= (5 - 10\sin\pi/5 \text{ cm}, -10\cos\pi/5 \text{ cm}, \pi/2 \text{ rad}), \\
q_{d5}(0) &= (5 - 10\cos\pi/10 \text{ cm}, 10\sin\pi/10 \text{ cm}, \pi/2 \text{ rad}).
\end{aligned}$$

The desired formation at $t = 0$ along with the desired trajectory for the geometric center of the pentagon is shown in the Figure 3.3. The graph was selected as the spanning tree shown in Figure 3.1 with edge set $E = \{(1,2),(2,3),(3,4),(4,5)\}$. The initial positions and orientations of the robots were randomly set to

$$\begin{aligned}
q_1(0) &= (2.37 \text{ cm}, 8 \text{ cm}, 0.0162 \text{ rad}), q_2(0) = (17.5 \text{ cm}, 6 \text{ cm}, 0.0218 \text{ rad}), \\
q_3(0) &= (2.06 \text{ cm}, -1.36 \text{ cm}, -0.0031 \text{ rad}), q_4(0) = (-9.9 \text{ cm}, -11.49 \text{ cm}, 0.0517 \text{ rad}), \\
q_5(0) &= (-4.45 \text{ cm}, 8.62 \text{ cm}, -0.0452 \text{ rad}).
\end{aligned}$$

The control gain in (3.16) was set to $\lambda_1 = I_5 \otimes \text{diag}(2, 2, 10)$ where I_k is the $k \times k$ identity matrix. Snapshots of the initial and final formations are given in Figure 3.4 showing that the desired

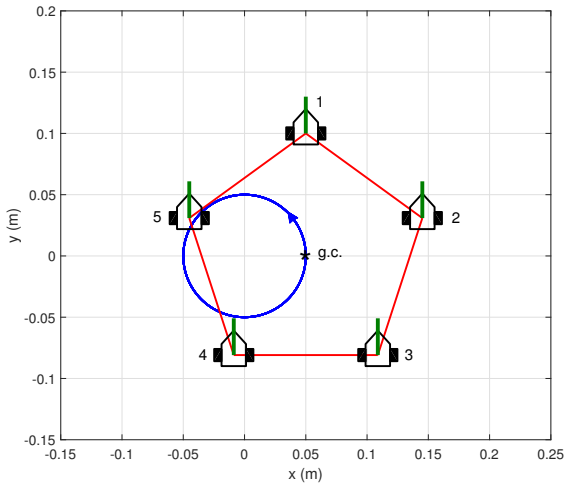

Figure 3.3. Experiment: Desired pentagon formation at $t = 0$ along with desired circular trajectory for the geometric center.

formation was successfully acquired from a random initial configuration. The path of each robot as they maneuver in formation is shown in Figure 3.5. Figure 3.6 shows the norm of all tracking and coordinations errors quickly converging to approximately zero. The errors are not exactly zero due to measurement noise and the sensor resolution. We can see from the errors that the desired pentagon formation is acquired after approximately 10 s while simultaneously maneuvering around the desired circular path. The control inputs are depicted in Figure 3.7, where one can see that $\eta_i(t) \to \eta_{di}$ as $t \to \infty$ for all i as expected. A video of the experiment can be seen via this link: `https://www.youtube.com/watch?v=4q_rSynUDjA`

3.4.2 Adaptive Dynamics Control Simulation

Since Robotarium does not allow the specification of actuator-level commands, a simulation conducted in MATLAB was used to demonstrate the performance of the adaptive dynamics controller from Section 3.3. The system parameters in (2.7) were set to $m_i = 3.6$ kg, $J_i = 0.0405$ kg-m^2, and $D_i = \text{diag}(0.3 \text{ kg/s}, 0.004 \text{ kg-m}^2/s)$ for $i = 1, ..., 5$. The desired formation maneuver was similar to the one in the experiment with exception of $\eta_{di} = (4 \text{ m/s}, 1 \text{ rad/s})$, $i = 1, ..., 5$ and

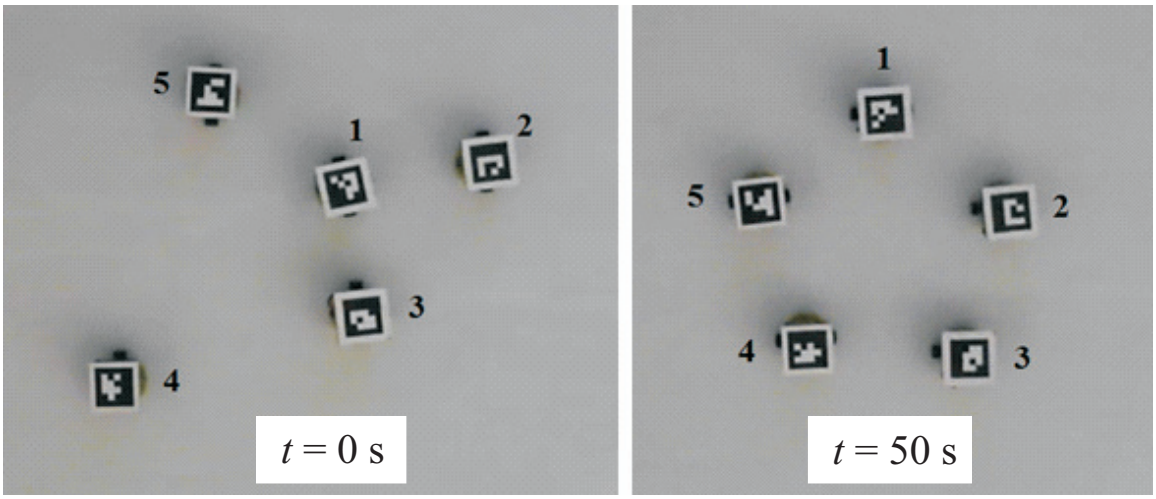

Figure 3.4. Experiment: Snapshots of the initial formation (left) and the formation when the experiment was stopped (right).

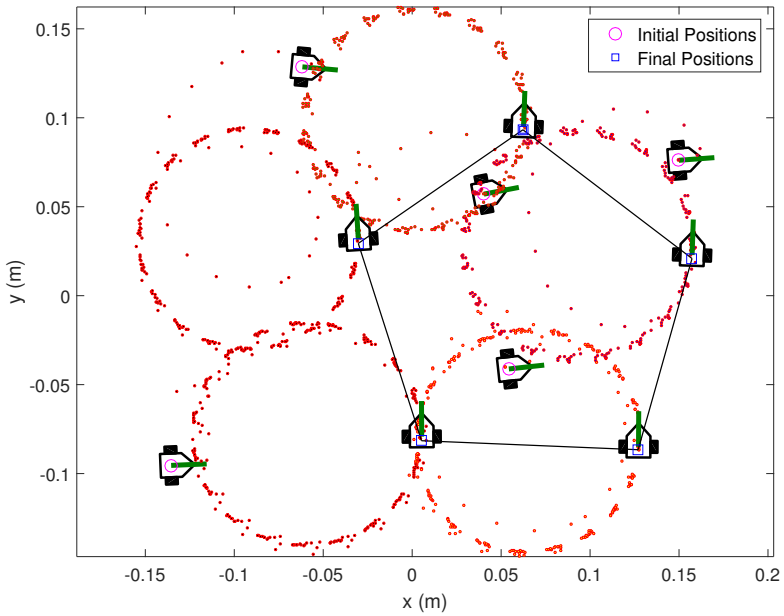

Figure 3.5. Experiment: Circular maneuver of each robot from the initial formation at $t = 0$ s to the formation at $t = 50$ s.

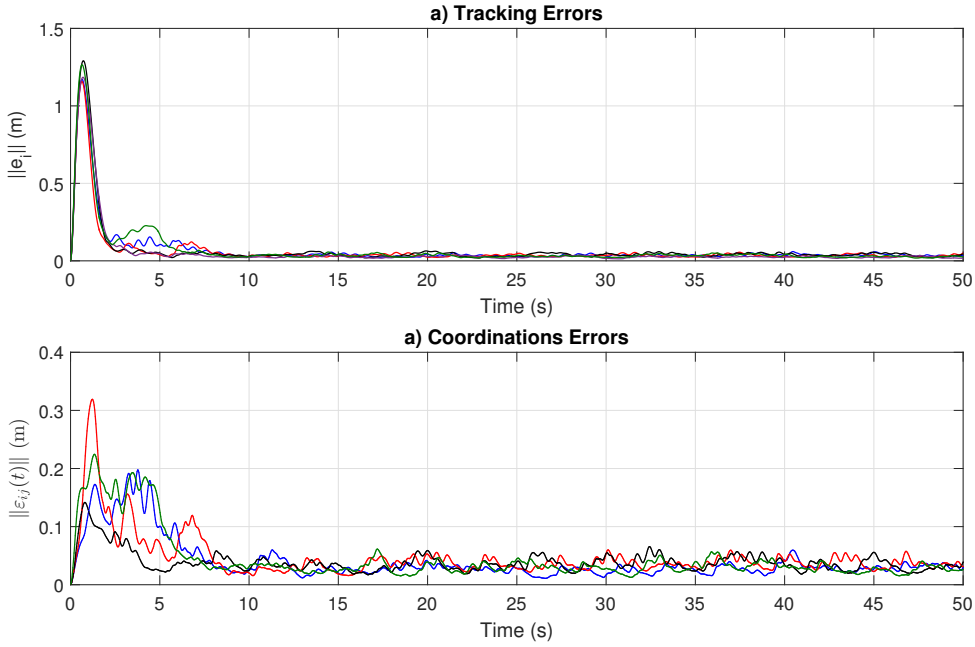

Figure 3.6. Experiment: a) Norm of the tracking errors, $\|e_i(t)\|$, $i = 1, .., 5$; b) norm of the coordination errors, $\|\varepsilon_{ij}(t)\|$, $(i, j) \in E$.

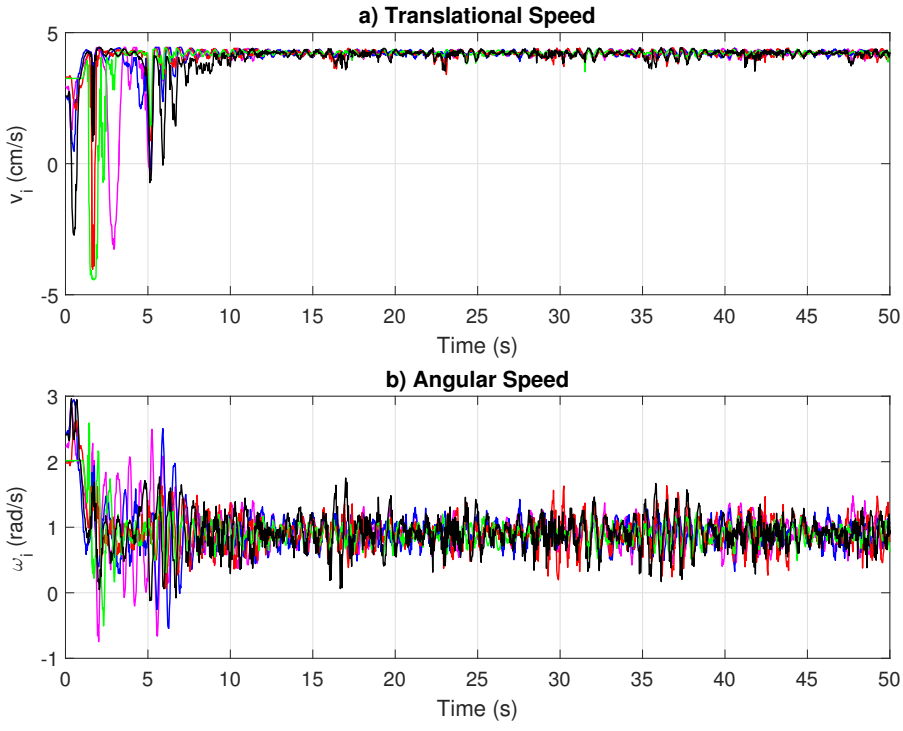

Figure 3.7. Experiment: Control input $\eta_i(t) = (v_i(t), \omega_i(t))$, $i = 1, \ldots, 5$.

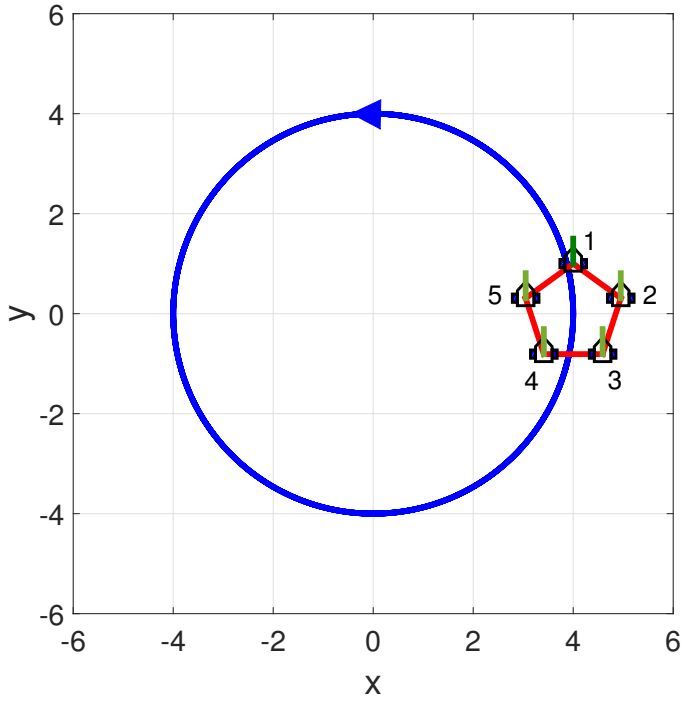

Figure 3.8. Simulation: Desired pentagon formation at $t = 0$ along with the desired circular trajectory for the geometric center.

the initial conditions

$$
\begin{aligned}
q_{d1}(0) &= (4\text{ m}, 1\text{ m}, \pi/2\text{ rad}), \quad q_{d2}(0) = (4 + \cos\pi/10\text{ m}, \sin\pi/10\text{ m}, \pi/2\text{ rad}), \\
q_{d3}(0) &= (4 + \sin\pi/5\text{ m}, -\cos\pi/5\text{ m}, \pi/2\text{ rad}), \\
q_{d4}(0) &= (4 - \sin\pi/5\text{ m}, -\cos\pi/5\text{ m}, \pi/2\text{ rad}), \\
q_{d5}(0) &= (4 - \cos\pi/10\text{ m}, \sin\pi/10\text{ m}, \pi/2\text{ rad}).
\end{aligned}
$$

The graph was set to the one in Figure 3.1. The desired formation at $t = 0$ along with the desired trajectory for the geometric center of the pentagon is shown in the Figure 3.8.

The initial conditions for the robots' position and orientation were randomly chosen as

$$\begin{aligned} q_1(0) &= (0.0940 \text{ m}, 1.3850 \text{ m}, 0.2600 \text{ rad}), \quad q_2(0) = (1.5735 \text{ m}, 0.1980 \text{ m}, 0.6210 \text{ rad}), \\ q_3(0) &= (1.000 \text{ m}, -1.0115 \text{ m}, 0.8475 \text{ rad}), \quad q_4(0) = (0.0500 \text{ m}, -0.1415 \text{ m}, 0.5260 \text{ rad}), \\ q_5(0) &= (-0.3845 \text{ m}, 0.9120 \text{ m}, 0.0305 \text{ rad}). \end{aligned}$$

The initial translational and angular speed of each robot was set to zero. All parameter estimates in (3.38) were randomly initialized to a value in the interval $(0, 1)$. The control and adaptation parameters were set to $\lambda_1 = 2I_{15}$, $\lambda_2 = 4I_{10}$, $\Gamma = 0.5I_{30}$, $c = 1$, and $\varrho = 3$.

Figure 3.9 shows the snapshots in time of the unicycle robots as they maneuver in formation. Only the trajectories of two robots are shown for illustration purposes. Figures 3.10 and 3.11 show the time evolution of $\|e_i(t)\|$, $i = 1, \ldots, 5$ and $\|\varepsilon_{ij}(t)\|$, $(i, j) \in E$, respectively. Despite the stability analysis of Section 3.3 proving the uniform ultimate boundedness of the errors, the simulation shows the errors converging to zero. This is not surprising since Lyapunov-type analyses are generally conservative. We can see from these results that after approximately 17.5 s the robots converge to the pentagon formation while maneuvering as a rigid body around the circle. Some of the parameter estimates for robot 1 are shown in Figure 3.12. The parameter estimates for the other robots had a similar behavior, converging to some constant values.[3]

In order to illustrate the benefit of the dynamics controller over a pure kinematic one, we also simulated the kinematic controller as described in Remark 5 with the same gain values for λ_1 and λ_2 used in the adaptive control simulation. Figure 3.13 shows the tracking and coordination errors of the kinematic controller. As one can see, the tracking errors do not converge to zero as they do in Figure 3.10. Since all tracking errors are converging to the same nonzero value in Figure 3.13, the coordination errors of the kinematic controller nevertheless converge to zero since they are simply the difference of the tracking errors (see (3.2)).

[3]Recall that adaptive control does not, *in general*, guarantee the convergence of the parameter estimates to their actual values [55] .

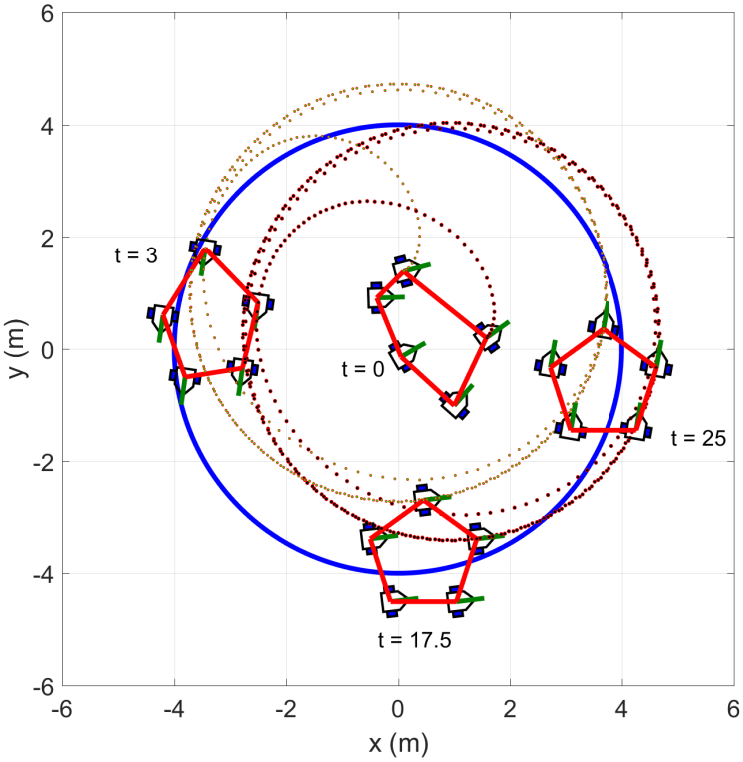

Figure 3.9. Simulation (Adaptive control): Snapshots in time of the formation maneuvering and the desired trajectory for the geometric center.

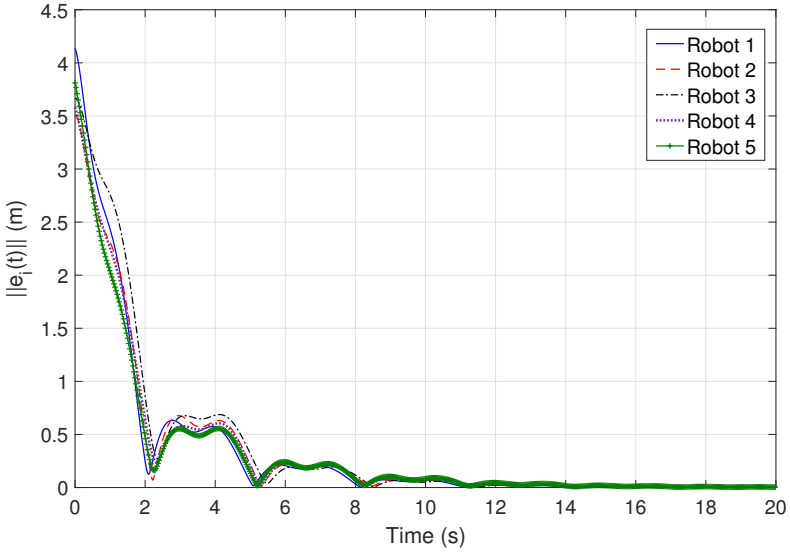

Figure 3.10. Simulation (Adaptive control): Norm of tracking errors, $\|e_i(t)\|$, $i = 1, .., 5$.

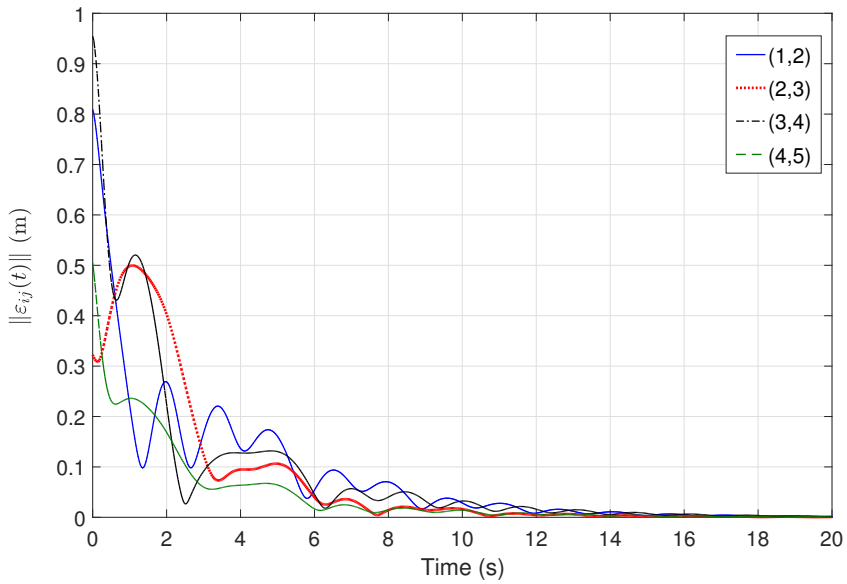

Figure 3.11. Simulation (Adaptive control): Norm of the coordination errors, $\|\varepsilon_{ij}(t)\|$, $(i,j) \in E$.

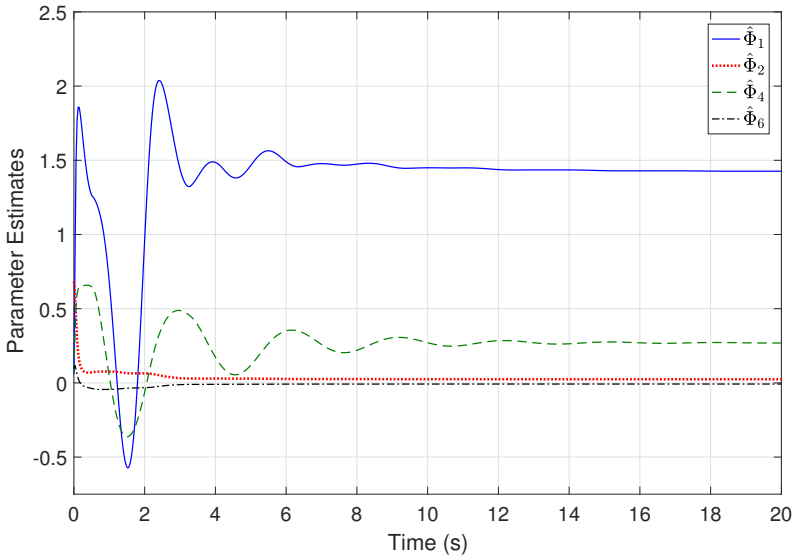

Figure 3.12. Simulation (Adaptive control): Sample of parameters estimates for robot 1.

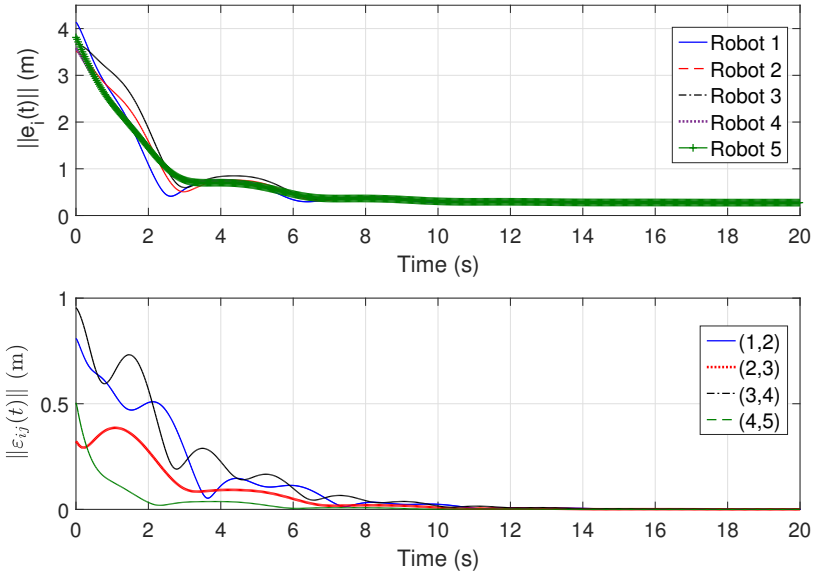

Figure 3.13. Simulation (Kinematic control): Tracking and coordination errors.

Chapter 4. Rigidity-Based Flocking Control

In this chapter, we present a solution to the distance-based formation maneuvering problem of multiple nonholonomic unicycle-type robots. The control law is designed at the kinematic level and is based on the rigidity properties of the graph modeling the sensing/control interactions among the robots. A simple input transformation is used to facilitate the control design by converting the nonholonomic model into the single-integrator equation. The resulting control ensures exponential convergence to the desired formation while the formation maneuvers according to a desired, time-varying translational velocity. An experimental implementation of the proposed control law is conducted on the Robotarium testbed [62].

4.1 Problem Statement

Consider that the agents' target formation is modeled by the framework $F^* = (G^*, q^*)$ where $G^* = (V^*, E^*)$, $\dim(V^*) = n$, $\dim(E^*) = a$, $p^* = [p_1^*, \ldots, p_n^*]$, and $p_i^* = [x_i^*, y_i^*]$. The fixed target distance separating the ith and jth agents is given by

$$d_{ij} = \left\|p_i^* - p_j^*\right\| > 0, \quad i, j \in V^*. \tag{4.1}$$

We assume F^* is constructed to be infinitesimally and minimally rigid. The actual formation of the agents is encoded by the framework $F(t) = (G^*, p(t))$ where $p = [p_1, \ldots, p_n]$ and $p_i = [x_i, y_i]$.

The statement of the control problem of this chapter is the following.

Flocking Problem: The agents need to acquire and maintain a pre-defined geometric shape in the plane while simultaneously moving with a given translational velocity. That is,

$$F(t) \to \mathrm{Iso}\,(F^*) \text{ as } t \to \infty, \tag{4.2}$$

which is equivalent to

$$\|p_i(t) - p_j(t)\| \to d_{ij} \text{ as } t \to \infty, \quad i, j \in V^* \tag{4.3}$$

due to the framework rigidity, and

$$\dot{p}_i(t) - v_0(t) \to 0 \text{ as } t \to \infty, \quad i = 1, ..., n \tag{4.4}$$

where $v_0 \in \mathbb{R}^2$ is any continuously differentiable function of time representing the desired translational velocity. We assume v_0 and $\dot{v}_0$ are bounded for all time.

The proposed control scheme assumes that the velocity $v_0(t)$ is known to all agents. This is not an overly restrictive assumption since in many cases this information is known beforehand and can pre-programmed into the agents' onboard computer.

4.2 Control Formulation

Before presenting the control scheme, we introduce several error variables. The relative position of agents i and j is defined as

$$\tilde{p}_{ij} = p_i - p_j, \tag{4.5}$$

while their distance error is captured by the variable [45]

$$z_{ij} = \|\tilde{p}_{ij}\|^2 - d_{ij}^2. \tag{4.6}$$

The vector of all z_{ij} for which $(i, j) \in E^*$ is defined as $z = [..., z_{ij}, ...] \in \mathbb{R}^a$, which is ordered as (1.2). Given that $\|\tilde{p}_{ij}\| \geq 0$, note that $z_{ij} = 0$ if and only if $\|\tilde{p}_{ij}\| = d_{ij}$. This means that when $z = 0$, the frameworks F and F^* are equivalent and therefore, $F = \text{Iso}(F^*)$ or $F = \text{Amb}(F^*)$. Finally, let

$$\tilde{\theta}_i = \theta_i - \theta_{di} \tag{4.7}$$

where θ_{di} denotes the desired heading direction, which is to be specified later.

Theorem 5 *Let the initial conditions for the distance errors be* $z(0) \in \Omega_1 \cap \Omega_2$

$$\begin{aligned} \Omega_1 &= \{z \in \mathbb{R}^a \mid \Lambda(F, F^*) \leq \delta\} \\ \Omega_2 &= \{z \in \mathbb{R}^a \mid dist(p, Iso(F)) < dist(p, Amb(F^*))\} \end{aligned} \tag{4.8}$$

where δ *is a sufficiently small positive constant. Then, the kinematic control law*

$$v_i = u_{ix}\cos\theta_i + u_{iy}\sin\theta_i \tag{4.9a}$$

$$\omega_i = -\beta_i\tilde{\theta}_i + \dot{\theta}_{di} \tag{4.9b}$$

$$u_i = \begin{bmatrix} u_{ix} \\ u_{iy} \end{bmatrix} = -k \sum_{j \in \mathcal{N}_i(E^*)} \tilde{p}_{ij} z_{ij} + v_0 \tag{4.9c}$$

$$\theta_{di} = \begin{cases} 0, & \text{if } u_{ix} = u_{iy} = 0 \\ atan2(u_{iy}, u_{ix}), & \text{otherwise,} \end{cases} \tag{4.9d}$$

where β_i *and* k *are positive control gains, ensures* $(z, \tilde{\theta}_i) = 0$ *for all* $i \in V^*$ *is exponentially stable and that (4.2) and (4.4) hold.*

Proof. We first decompose (2.6) as follows

$$\dot{p}_i = \begin{bmatrix} v_i\cos\theta_i \\ v_i\sin\theta_i \end{bmatrix} \tag{4.10}$$

$$\dot{\theta}_i = \omega_i. \tag{4.11}$$

Using (4.7), (4.9a), and (4.9d) in (4.10), one arrives at

$$\dot{p}_i = B(\tilde{\theta}_i)u_i. \tag{4.12}$$

where

$$B(\tilde{\theta}_i) = \begin{bmatrix} \cos^2\tilde{\theta}_i & -\frac{1}{2}\sin 2\tilde{\theta}_i \\ \frac{1}{2}\sin 2\tilde{\theta}_i & \cos^2\tilde{\theta}_i \end{bmatrix} \tag{4.13}$$

Now, taking the time of derivative of (4.6) gives

$$\dot{z}_{ij} = \frac{d}{dt}\left(\tilde{p}_{ij}^{\intercal}\tilde{p}_{ij}\right) = 2\tilde{p}_{ij}^{\intercal}\left(B(\tilde{\theta}_i)u_i - B(\tilde{\theta}_j)u_j\right), \tag{4.14}$$

which can be rewritten in the following vector form

$$\dot{z} = 2R(p)\mathbf{B}(\tilde{\theta})u \tag{4.15}$$

where (3.7) was used, $\mathbf{B}(\tilde{\theta}) = \text{diag}\Big(B(\tilde{\theta}_1), ..., B(\tilde{\theta}_n)\Big) \in \mathbb{R}^{2n\times 2n}$, $\tilde{\theta} = \Big[\tilde{\theta}_1, \ldots, \tilde{\theta}_n\Big] \in \mathbb{R}^n$, and $u = [u_1, \ldots, u_n] \in \mathbb{R}^{2n}$. Likewise, (4.9c) can be rewritten as

$$u = -kR^{\intercal}(p)z + 1_n \otimes v_0. \tag{4.16}$$

After substituting (4.16) into (4.15), we obtain

$$\dot{z} = -2kR(p)\mathbf{B}(\tilde{\theta})R^{\intercal}(p)z + 2R(p)\mathbf{B}(\tilde{\theta})(1_n \otimes v_0). \tag{4.17}$$

Next, after taking the derivative of (4.7) and substituting (4.11) and (4.9b), we obtain

$$\dot{\tilde{\theta}}_i = -\beta_i\tilde{\theta}_i, \tag{4.18}$$

which indicates that $\tilde{\theta}_i = 0$, $\forall i \in V^*$ is exponentially stable.

Our overall closed-loop system includes two interconnected subsystems (4.17) and (4.18), which are in the form of (1.6). Now, we show that (4.17) is input-to-state stable with respect to $\tilde{\theta}$ by

using Theorem 1. Consider the Lyapunov function candidate

$$V = \frac{1}{4} \sum_{(i,j) \in E^*} z_{ij}^2 = \frac{1}{4} z^\intercal z. \tag{4.19}$$

The derivative of (4.19) along (4.17) is given by

$$\dot{V} = -k z^\intercal R(p) \mathbf{B}(\tilde{\theta}) R^\intercal(p) z + z^\intercal R(p) \mathbf{B}(\tilde{\theta})(1_n \otimes v_0). \tag{4.20}$$

When $\tilde{\theta} = 0$, $\mathbf{B}(\tilde{\theta}) = I_{2n \times 2n}$ and (4.20) becomes

$$\dot{V} = -k z^\intercal R(p) R^\intercal(p) z \tag{4.21}$$

upon application of Lemma 2. Given that F^* and $F(t)$ have the same edge set and F^* is minimally rigid by design, then $F(t)$ is minimally rigid for all $t \geq 0$. Moreover, from Lemma 1 and the fact that F^* is infinitesimally rigid, we know $F(t)$ is infinitesimally rigid for $z(t) \in \Omega_1$. Therefore, $R(p)$ has full row rank and

$$\dot{V} \leq -k \underline{\lambda} z^\intercal z \quad \text{for} \quad z(t) \in \Omega_1 \tag{4.22}$$

where $\underline{\lambda} = \inf_t \lambda_{\min}(RR^\intercal) > 0$ and $\lambda_{\min}$ represents the minimum eigenvalue. From (4.22), we know that $\dot{V}(t) \leq 0$ for all $t \geq 0$, which implies that $V(t) \leq V(0)$ for all $t > 0$. Therefore, since $z(t) \in \Omega_1$ is equivalent to $z(t) \in \{z \in \mathbb{R}^{2n} \mid V(z) \leq c\}$ according to Lemma 2 of [12], a sufficient condition for (4.22) is given by

$$\dot{V} \leq -4k \underline{\lambda} V \quad \text{for} \quad z(0) \in \Omega_1. \tag{4.23}$$

From (4.23), we know that $z = 0$ is exponentially stable for $z(0) \in \Omega_1$ [40], which is equivalent to the input-to-state stability of (4.17) with respect to $\tilde{\theta}$. Therefore, $[z, \tilde{\theta}] = 0$ is a locally stable equilibrium point of the interconnected system by Theorem 2.

The exponential stability of $z = 0$ infers one of two possible occurrences: $F(t) \to \text{Iso}(F^*)$ or $F(t) \to \text{Amb}(F^*)$ as $t \to \infty$. Since the initial condition is such that $z(0) \in \Omega_1 \cap \Omega_2$, then we have

from (4.8) that

$$\mathrm{dist}(q(0), \mathrm{Iso}(F^*(0))) < \mathrm{dist}(q(0), \mathrm{Amb}(F^*(0))). \tag{4.24}$$

It follows from this condition that the energy function (4.19) would necessarily have to increase for a certain time interval for $F(t) \to \mathrm{Amb}(F^*)$ as $t \to \infty$ to occur. This is however contradictory to the fact that $V(t)$ is nonincreasing for all time. Thus, we conclude that $F(t) \to \mathrm{Iso}(F^*)$ as $t \to \infty$ for $z(0) \in \Omega_1 \cap \Omega_2$.

Since $z(t)$ is bounded, we know from (4.6) that $\tilde{p}_{ij}(t)$, $(i,j) \in E^*$ is bounded. Therefore, since $z(t) \to 0$ and $\tilde{\theta}(t) \to 0$ as $t \to \infty$, we know from (4.9c) and (4.12) that $\dot{p}_i(t) - v_0(t) \to 0$ as $t \to \infty$ for $\forall i \in V^*$. ■

Remark 6 *The time derivative of (4.9d), which is needed in (4.9b), can be calculated as follows*

$$\dot{\theta}_{di} = \begin{cases} 0, & \text{if } u_{ix} = u_{iy} = 0 \\ \frac{-u_{iy}}{u_{ix}^2+u_{iy}^2}\dot{u}_{ix} + \frac{u_{ix}}{u_{ix}^2+u_{iy}^2}\dot{u}_{iy}, & \text{otherwise} \end{cases} \tag{4.25}$$

where

$$\dot{u}_i = -k \sum_{j \in \mathcal{N}_i(E^*)} \left(z_{ij} + 2\tilde{p}_{ij}\tilde{p}_{ij}^{\mathsf{T}}\right)(u_i - u_j) + \dot{v}_0 \tag{4.26}$$

and (4.12) and (4.14) were used.

Remark 7 *The control (4.9) is time invariant and discontinuous, which is expected by Brockett's condition for stabilization of nonholonomic systems [7]. Interestingly, the experimental study in [42] has shown that such controllers can yield better performance than time-varying, continuous controls if carefully implemented on unicycle-type robots.*

4.3 Experimental Results

An experiments with five robots were again conducted on the Robotarium system. The desired formation F^* was set to a regular pentagon, which was made infinitesimally and minimally rigid by introducing seven edges such that $E^* = \{(1,2),(1,3),(1,4),(1,5),(2,3),(3,4),(4,5)\}$. The desired distances between all robots were given by $d_{12} = d_{23} = d_{34} = d_{45} = d_{15} = \lambda\sqrt{2(1-c_1)}$ and

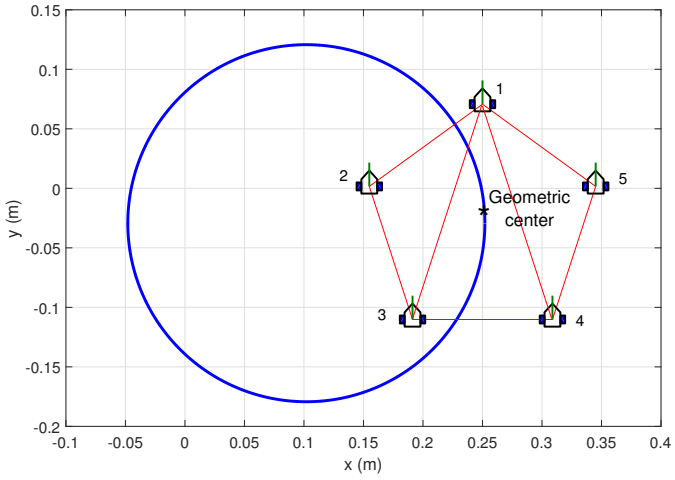

Figure 4.1. Desired pentagon formation along with desired circular trajectory for the geometric center.

$d_{13} = d_{14} = \lambda\sqrt{2(1+c_2)}$ where $\lambda = 0.1$ m, $s_1 = \sin\frac{2\pi}{5}$, $s_2 = \sin\frac{4\pi}{5}$, $c_1 = \cos\frac{2\pi}{5}$, and $c_2 = \cos\frac{\pi}{5}$. The formation was required to move as a virtual rigid body around a circle. To this end, the desired flocking velocity was chosen as $v_f(t) = [-r\varpi\sin\varpi t, r\varpi\cos\varpi t]$ m/s where $r = 0.15$ m is the radius for the circular trajectory and $\varpi = 0.3$ rad/s. Figure 4.1 depicts the desired formation and desired maneuver. The initial positions and orientations of the robots were randomly selected. The control gains in (4.9b) and (4.9c) were set to $\beta_i = 10$, $i = 1, ..., 5$, and $k = 6$.

Snapshots of the formation at $t = 0$ s and $t = 32$ s are given in Figure 4.2 showing that the desired formation was successfully acquired from the random initial configuration. The path of the geometric center of the formation as it maneuvered in the circle is shown in Figure 4.3. Figure 4.4 shows the inter-agent distance errors and heading angle errors quickly converging to approximately zero. The errors are not exactly zero due to measurement noise and the sensor resolution. We can observe from the errors that the desired formation is acquired after approximately 25 s. The control inputs are depicted in Figure 4.5, where one can see that $v_i(t) \to r\varpi = 4.5$ cm/s as $t \to \infty$ for all i. The steady-state values for $\omega_i(t)$, $i = 1, ..., 5$, are approximately 0.5 rad/s rather than the expected value of $\varpi = 0.3$ rad/s. This can be explained from (4.9b) by the facts that a) the term $\beta_i\tilde{\theta}_i(t)$ does not approach zero as $t \to \infty$ due to the small steady-state offset and fluctuation in $\tilde{\theta}_i$, and b) the term $\dot{\theta}_{di}(t)$ does not approach 0.3 as $t \to \infty$ due to the manner in which (4.25) is calculated. Also,

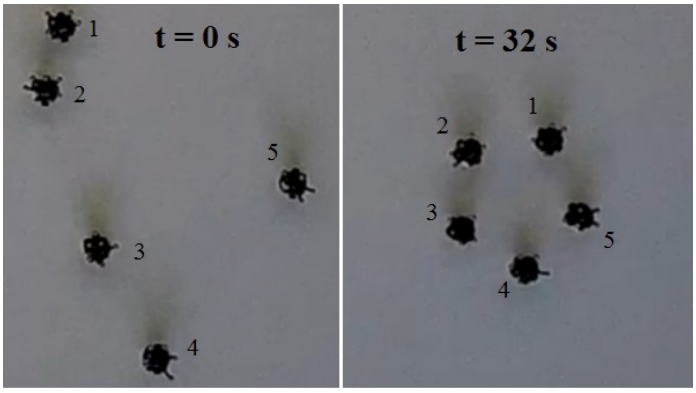

Figure 4.2. Snapshots of the initial formation (left) and the formation when the desired formation was acquired (right).

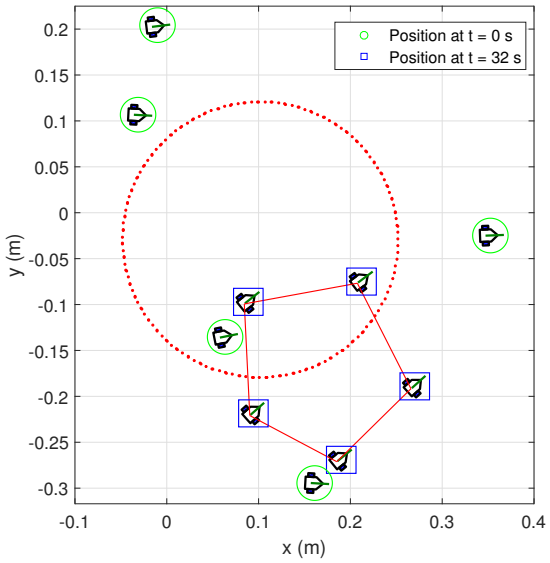

Figure 4.3. Circular maneuver of the robots from the initial formation.

notice from Figure 4.5 that the Robotarium testbed limits the robot's linear velocity to ± 10 cm/s.

A video of the experiment can be seen in `https://www.youtube.com/watch?v=2EV_SUpvsrk`.

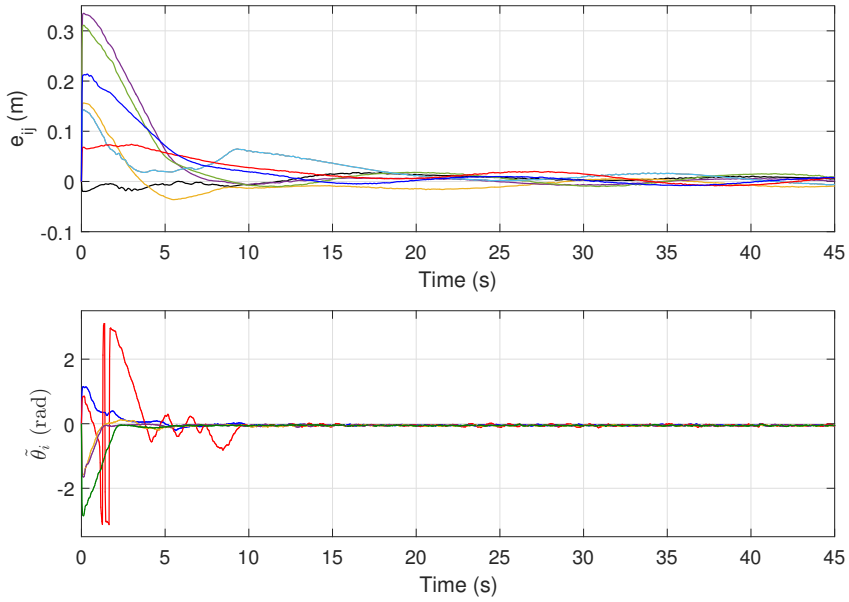

Figure 4.4. Distance errors, $e_{ij}(t)$, $i, j \in V^*$ (top) and heading angle errors, $\tilde{\theta}_i(t)$, $i = 1, ..., 5$ (bottom).

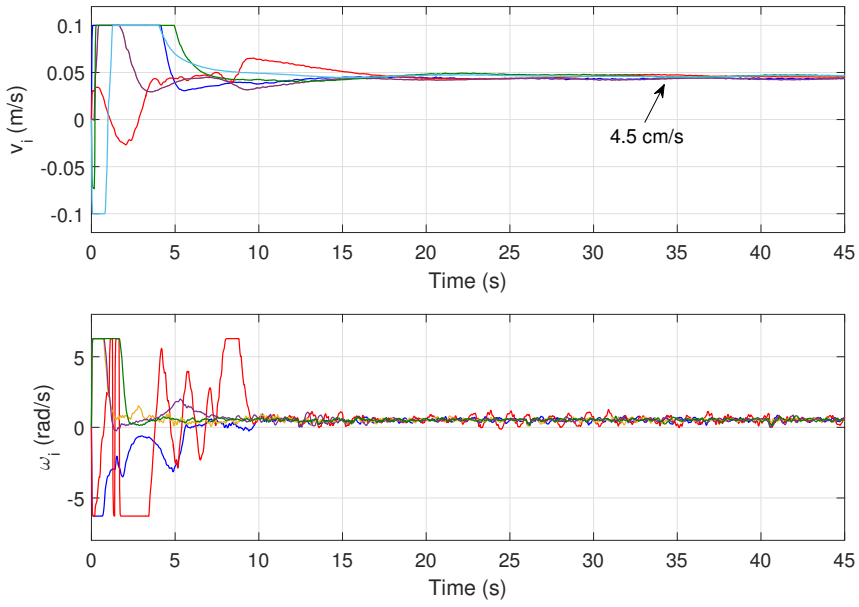

Figure 4.5. Control inputs $\eta_i(t) = [v_i(t), \omega_i(t)]$, $i = 1, \ldots, 5$.

Chapter 5. Flocking Control with Limited Information

In this chapter, we present solutions to the distance-based flocking problem. Like in Chapter 4, we design kinematic-level control laws based on the rigidity properties of the graph. The challenge here is that the translational velocity is assumed to be known only to a subset of agents in the formation. As a result, the controls will include a distributed observer to identify the unknown velocities.

5.1 Problem Statement

A formal statement of the problem tackled in this chapter is given next.

Flocking Problem II: This problem is similar to the flocking problem described in Section 4.1, but with the constraint that only agents $i \in V_0$, where $V_0 \subset V^*$ is a nonempty subset, have direct access to v_0. We assume $v_0(t)$ is any bounded, continuously differentiable function of time such that $\|\dot{v}_0\| \leq \gamma$ where γ is a known positive constant. Thus, the control objective is to ensure that both (4.2) and (4.4) hold.

5.2 Flocking Control Formulation

The control law that solves the flocking problem stated above is given in the following theorem.

Theorem 6 *Let the initial conditions for the distance errors be $z(0) \in \Omega_1 \cap \Omega_2$ where Ω_1 and Ω_2 were defined in (4.8). Then, the kinematic control law*

$$v_i = u_{ix}\cos\theta_i + u_{iy}\sin\theta_i \tag{5.1}$$

$$\omega_i = -\beta_i\tilde{\theta}_i + \dot{\theta}_{id} \tag{5.2}$$

$$u_i = \begin{bmatrix} u_{ix} \\ u_{iy} \end{bmatrix} = -k\sum_{j\in\mathcal{N}_i(E^*)} \tilde{p}_{ij}z_{ij} + \hat{v}_{fi} \tag{5.3}$$

$$\dot{\hat{v}}_{fi} = -\alpha sgn\left(\sum_{j\in\mathcal{N}_i(E^*)} (\hat{v}_{fi} - \hat{v}_{fj}) \; - b_i(\hat{v}_{fi} - v_0)\right) \tag{5.4}$$

$$\theta_{id} = \begin{cases} 0, & \text{if } u_{ix} = u_{iy} = 0 \\ atan2(u_{iy}, u_{ix}), & \text{otherwise,} \end{cases} \tag{5.5}$$

where $\beta_i, k > 0$ are control gains,

$$b_i = \begin{cases} 1, & \textit{if } i \in V_0 \\ 0, & \textit{otherwise,} \end{cases}, \tag{5.6}$$

$\alpha > \gamma$ is an observer gain, and $sgn(\cdot)$ is the standard signum function defined as

$$sgn\,(x) = \begin{cases} 1 & \textit{for } x > 0 \\ 0 & \textit{for } x = 0 \\ -1 & \textit{for } x < 0, \end{cases} \tag{5.7}$$

ensures $(z, \tilde{\theta}_i) = 0$ for all $i \in V^*$ is exponentially stable and that (4.2) and (4.4) hold.

Proof. The proof of this theorem will follow similar arguments to those used in the proof of Theorem 5. From (5.3), we have that

$$u = -kR^{\intercal}(p)z + \hat{v}_f \tag{5.8}$$

where $\hat{v}_f = [\hat{v}_{f1}, ..., \hat{v}_{fn}] \in \mathbb{R}^{2n}$. Let $\tilde{v}_{fi} = \hat{v}_{fi} - v_0$ denote the flocking velocity estimation error for agent i. If $\tilde{v}_f = [\tilde{v}_{f1}, ..., \tilde{v}_{fn}] \in \mathbb{R}^{2n}$, then

$$\tilde{v}_f = \hat{v}_f - \mathbf{1}_n \otimes v_0. \tag{5.9}$$

As part of this proof, we will show that (5.4) guarantees $\tilde{v}_f(t) \to 0$ as $t \to \infty$.

After substituting (5.8) into (4.15), we get the closed-loop system

$$\dot{z} = -2kR(p)\mathbf{B}(\tilde{\theta})R^{\intercal}(p)z + 2R(p)\mathbf{B}(\tilde{\theta})\hat{v}_f. \tag{5.10}$$

Using (5.9) in (5.10) yields

$$\dot{z} = -2kR(p)\mathbf{B}(\tilde{\theta})R^{\intercal}(p)z + 2R(p)\mathbf{B}(\tilde{\theta})(\tilde{v}_f + \mathbf{1}_n \otimes v_0). \tag{5.11}$$

We now turn our attention to deriving the dynamics of the estimation error. First, notice that

$$\sum_{j \in N_i(E^*)} (\hat{v}_{fi} - \hat{v}_{fj}) = \sum_{j=1}^{n} a_{ij}(\hat{v}_{fi} - \hat{v}_{fj}), \tag{5.12}$$

where a_{ij} are the elements of the adjacency matrix A. Taking the time derivative of (5.9) and substituting (5.4) gives

$$\begin{aligned} \dot{\tilde{v}}_f &= -\alpha \text{sgn}\left((\mathcal{L} \otimes I_2)\tilde{v}_f - (\mathcal{B} \otimes I_2)\tilde{v}_f\right) - \mathbf{1}_n \otimes \dot{v}_0 \\ &= -\alpha \text{sgn}\left((\mathcal{M} \otimes I_2)\tilde{v}_f\right) - \mathbf{1}_n \otimes \dot{v}_0 \end{aligned} \tag{5.13}$$

where we used the fact that $\hat{v}_{fi} - \hat{v}_{fj} = \tilde{v}_{fi} - \tilde{v}_{fj}$, $\mathcal{B} :=\text{diag}(b_1, ..., b_n)$, $\mathcal{L}$ is the Laplacian matrix, and $\mathcal{M} := \mathcal{L} + \mathcal{B}$.

Our overall closed-loop system is composed of three interconnected subsystems: (5.11), (5.13), and (4.18). This interconnected system is in the form of (1.6) with $y = [\tilde{v}_f, \tilde{\theta}]$. Therefore, we need to show that (5.11) is input-to-state stable with respect to $[\tilde{v}_f, \tilde{\theta}]$.

Taking the derivative (4.19) along (5.11) yields

$$\dot{V} = -kz^{\intercal}R(p)\mathbf{B}(\tilde{\theta})R^{\intercal}(p)z + z^{\intercal}R(p)\mathbf{B}(\tilde{\theta})(\tilde{v}_f + \mathbf{1}_n \otimes v_0). \tag{5.14}$$

After setting $[\tilde{v}_f, \tilde{\theta}] = 0$ in (5.14), we obtain (4.21). We can now follow the proof of Theorem 5 to conclude that (5.11) is input-to-state stable with respect to $[\tilde{v}_f, \tilde{\theta}]$.

Next, we prove that $\tilde{v}_f = 0$ is a stable equilibrium point of (5.13). Since the graph of a rigid framework is always connected, we know that G^* is connected. Therefore, we know from Lemma

3 of [35] that $\mathcal{M}$ is positive definite in (5.13). Consider the positive definite Lyapunov function

$$W = \frac{1}{2}\tilde{v}_f^{\intercal}(\mathcal{M} \otimes I_2)\tilde{v}_f. \tag{5.15}$$

The time derivative of W along (5.13) is given by

$$\begin{aligned}
\dot{W} &= \tilde{v}_f^{\intercal}(\mathcal{M} \otimes I_2)(-\alpha \text{sgn}\left((\mathcal{M} \otimes I_2)\tilde{v}_f\right) - \mathbf{1_n} \otimes \dot{v}_0) \\
&= -\alpha \tilde{v}_f^{\intercal}(\mathcal{M} \otimes I_2)\text{sgn}((\mathcal{M} \otimes I_2)\tilde{v}_f) - \tilde{v}_f^{\intercal}(\mathcal{M} \otimes I_2)(\mathbf{1_n} \otimes \dot{v}_0) \\
&= -\alpha \left\|(\mathcal{M} \otimes I_2)\tilde{v}_f\right\|_1 - (\mathbf{1_n} \otimes \dot{v}_0)^{\intercal}(\mathcal{M} \otimes I_2)\tilde{v}_f \\
&= -\alpha \left\|(\mathcal{M} \otimes I_2)\tilde{v}_f\right\|_1 + \dot{v}_0^{\top} \sum_{i=1}^{2n} \left[(M \otimes I_2)\, \tilde{v}_f\right]_i \\
&\leq -\alpha \left\|(\mathcal{M} \otimes I_2)\tilde{v}_f\right\|_1 + \left\|\dot{v}_0\right\|_1 \left\|(\mathcal{M} \otimes I_2)\tilde{v}_f\right\|_1 \\
&\leq -(\alpha - \gamma) \left\|(\mathcal{M} \otimes I_2)\tilde{v}_f\right\|_1
\end{aligned} \tag{5.16}$$

where $\|\cdot\|_1$ denotes the 1-norm. For $\alpha > \gamma$, $\dot{W}$ is negative definite and therefore $\tilde{v}_f = 0$ is asymptotically stable.

Since we already know that $\tilde{\theta} = 0$ is an exponentially stable equilibrium of (4.18), we can invoke Theorem 2 to claim that $(z, \tilde{v}_f, \tilde{\theta}) = 0$ is an asymptotically stable equilibrium of the interconnected system.

We again follow the arguments of the proof of Theorem 5 to show that (4.2) holds for $z(0) \in \Omega_1 \cap \Omega_2$.

Since $z(t)$ is bounded, we know from (4.6) that $\tilde{p}_{ij}$, $(i,j) \in E^*$ is bounded. Therefore, since $z(t) \to 0$ as $t \to \infty$, we know from (5.3) and (4.12) that $\dot{p}_i(t) - v_0(t) \to 0$ as $t \to \infty$ for $\forall i \in V^*$. ■

Remark 8 *The form of (5.4) is inspired by multi–agent consensus algorithms in [64] and [65]. The premise behind the observer is that agents that do not have direct access to v_0 can acquire this information from its neighbors since the graph modeling the communication network is connected. Note that the observer (5.4) can accommodate a leader-follower strategy (only one agent has access to v_0) as well as the general case where the velocity information exchange happens between any*

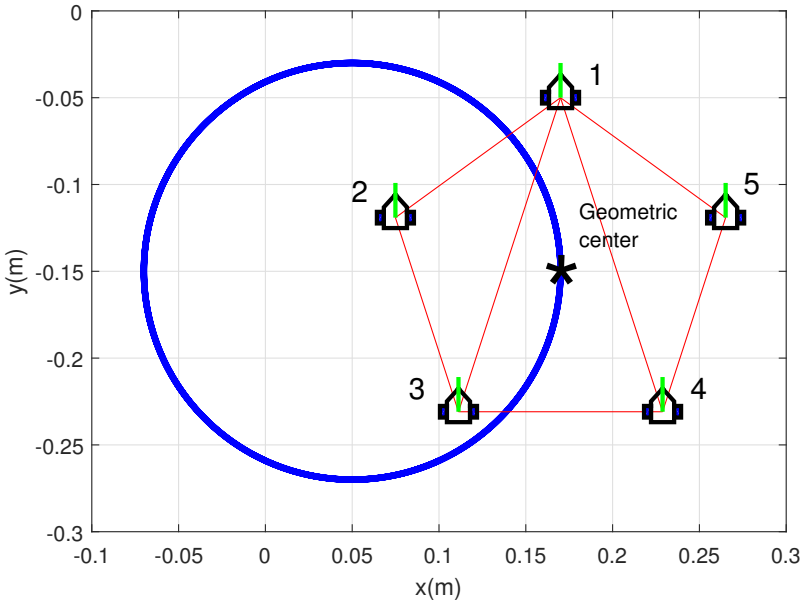

Figure 5.1. Desired pentagon formation along with desired circular trajectory for the geometric center.

two agents.

5.3 Experimental Results

The same experimental parameters described in Section 4.3 were used here. We set agent 1 to be the only one with access to the desired flocking velocity. As a result, b_i in (5.4) became

$$b_i = \begin{cases} 1, & \text{if } i = 1 \\ 0, & \text{otherwise.} \end{cases}$$

The control gains in (5.2) and (5.3) were set to $\beta_i = 10$, $i = 1, ..., 5$, and $k = 6$. The flocking velocity estimates were initialized to zero, i.e., $\hat{v}_{fi}(0) = 0$, $i = 1, ..., 5$. The observer gain in (5.4) was chosen as $\alpha = 0.05$, which satisfies the condition $\alpha > \gamma = r\varpi = 0.045$.

Snapshots of the formation at $t = 0$ s and $t = 32$ s are given in Figure 5.2 showing that the desired formation was successfully acquired from the random initial configuration. The path of the geometric center of the formation as it maneuvered in the circle is shown in Figure 5.3. Figure 5.4 shows the inter-agent distance errors, heading angle errors, and velocity estimation

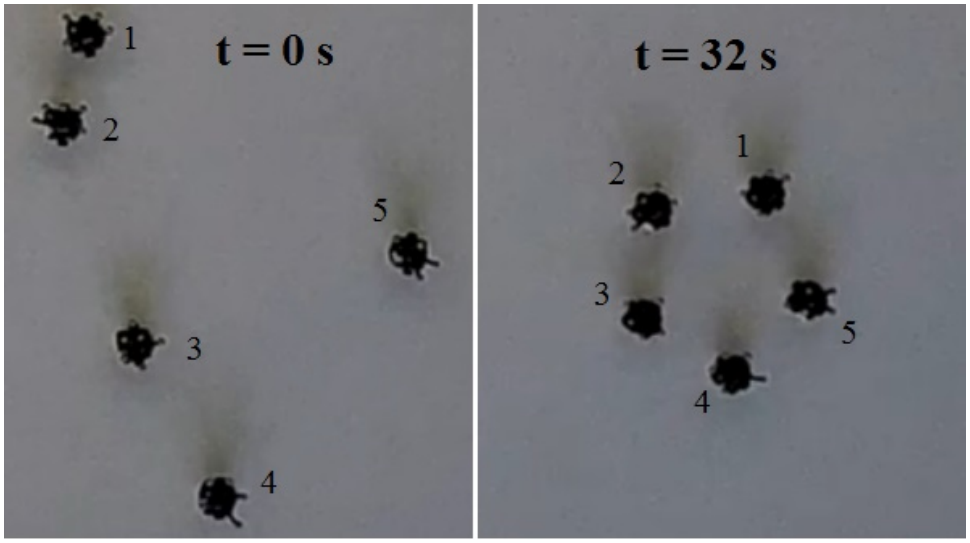

Figure 5.2. Snapshots of the initial formation (left) and the formation when the desired formation was acquired (right).

errors quickly converging to zero. We can observe from the errors that the desired formation is acquired after approximately 15 s. The control inputs are depicted in Figure 5.5, where one can see that $v_i(t) \to r\varpi = 4.5$ cm/s as $t \to \infty$ for all i. A video of the experiment can be seen in `https://www.youtube.com/edit?o=U&video_id=nujX1QsVUJI`.

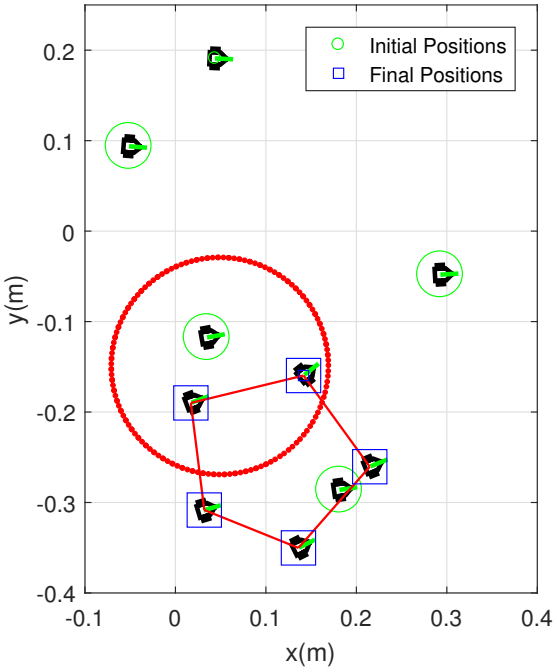

Figure 5.3. Circular maneuver of the robots from the initial formation.

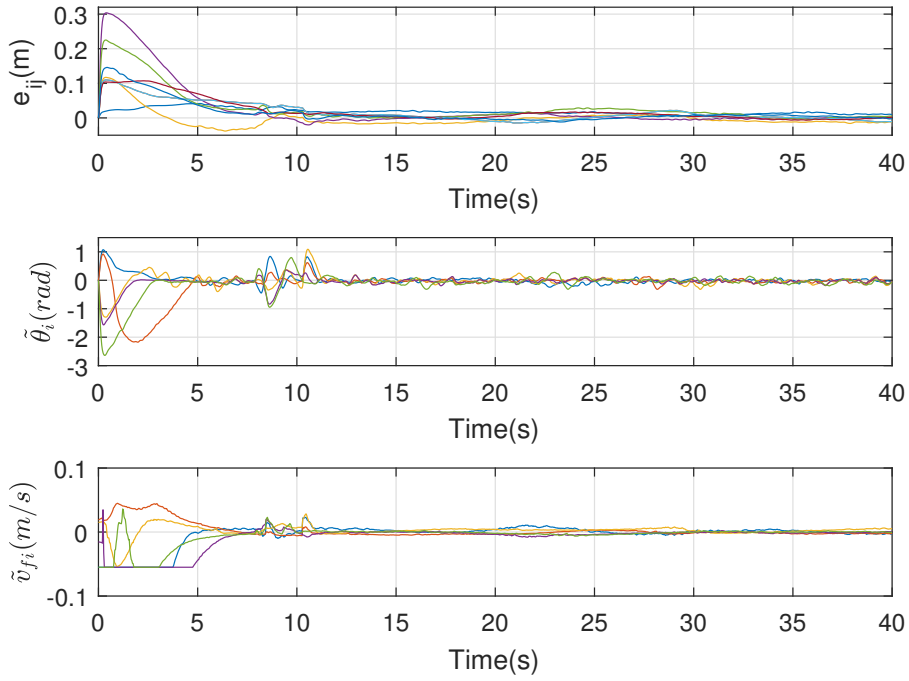

Figure 5.4. Distance errors, $e_{ij}(t)$, $i, j \in V^*$ (top), heading angle errors, $\tilde{\theta}_i(t)$, and velocity estimation errors, $\tilde{v}_{fi}$, $i = 1, ..., 5$.

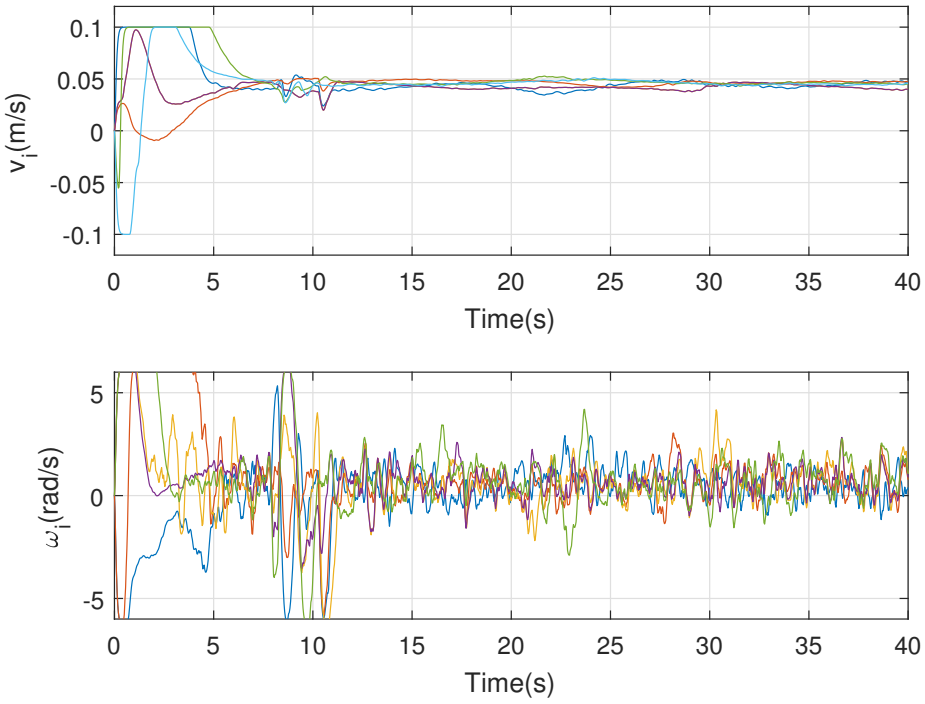

Figure 5.5. Control inputs $\eta_i(t) = [v_i(t), \omega_i(t)]$, $i = 1, \ldots, 5$.

Chapter 6. Conclusions

This dissertation introduced solutions to several formation control problems for nonholonomic robots. The key properties of the results in Chapter 3 were the use of a spanning tree to model the inter-robot coordination graph, the use of a leader-follower type strategy motivated by the spanning tree, and the judicious use of tracking errors and coordination errors to quantify the formation maneuvering control objective and decentralize the control system. A Lyapunov-based control law was designed that ensured that the formation maneuvering task is achieved in the least squares sense. Backstepping was used to extend the kinematic control to the dynamic case with parametric uncertainty. The kinematic control law was successfully implemented on the Robotarium testbed while a simulation demonstrated the model-based and adaptive controllers. The proposed formation controller does not include a collision avoidance strategy. However, one can incorporate the collision avoidance method from [44] since it only modifies the desired trajectories of robots at risk of colliding without interfering with the stability properties of the control.

Chapter 4 demonstrated how the distance-based flocking controller, originally designed for single-integrator models using rigid graph theory, can be applied to nonholonomic kinematic agents. An input transformation along with Lyapunov and input-to-state stability analyses showed that the proposed control ensures exponential convergence to the desired formation while maneuvering according to the desired translational velocity. An experimental validation of the formation control scheme was presented

Finally, in Chapter 5, we extended the distance-based flocking controller of Chapter 4 to the case where the flocking velocity is only known by some of the agents in the formation. Velocity matching was achieved by using a consensus-type velocity observer that exploits the connectivity of the formation graph.

All controllers were successfully validated either by simulation or by experimentation on the Robotarium testbed using unicycle-type robotic vehicles.

References

[1] Anderson, B.D.O., C. Yu, B. Fidan, and J. M. Hendrickx, "Rigid graph control architectures for autonomous formations," IEEE Control Systems Mag., 28(6), pp. 48-63, 2008.

[2] Asimow, L. and B. Roth, "The Rigidity of Graphs II," J. Math. Anal. Appl., 68(1), pp. 171-190, 1979.

[3] Borowska, J., L.Lacinska and J.Rychlewska, "A System of Linear Recurrence Equations For Determinant of Pentadiagonal Matrix," J. Appl. Math. Comp. Mech., 13(2), pp. 5-12, 2014.

[4] Aspnes, J., J. Egen, D.K. Goldenberg, A.S. Morse, W. Whiteley, Y.R. Yang, B.D.O. Anderson, and P.N. Belhumeur, "A Theory of Network Localization," IEEE Trans. Mob. Comput., 5(12), pp. 1663-1678, 2006.

[5] Bai, H., M. Arcak, and J.T. Wen, "Using Orientation Agreement to Achieve Planar Rigid Formation," Proc. Amer. Control Conf., pp. 753-758, Seattle, WA, 2008.

[6] Baillieul, J. and A. Suri, "Information Patterns and Hedging Brockett's Theorem in Controlling Vehicle Formations," Proc. IEEE Conf. Dec. Contr., pp. 556-563, Maui, HI, USA, 2003.

[7] Brockett, R., Asymtotic Stability and Feedback Stabilization, Boston, MA: Birkhauser, 1983.

[8] Cai, Z., M.S. de Queiroz, and D.M. Dawson, "A Sufficiently Smooth Projection Operator," IEEE Trans. Autom. Contr., 51(1), pp.135-139, 2006.

[9] Cai, X., and M. de Queiroz, "Multi-Agent Formation Maneuvering and Target Interception with Double-Integrator Model," Proc. Amer. Control Conf., pp. 287-292, Portland, OR, 2014.

[10] Cai, X., and M. de Queiroz, "Rigidity-Based Stabilization of Multi-Agent Formations," ASME J. Dyn. Syst., Measur., Contr., 136(1), Paper 014502, 2014.

[11] Cai, X., and M. de Queiroz, "Formation Maneuvering and Target Interception for Multi-Agent Systems via Rigid Graphs," Asian J. Contr., 17(4), pp. 1174-1186, 2015.

[12] Cai, X., and M. de Queiroz, "Adaptive Rigidity-Based Formation Control for Multi-Robotic Vehicles with Dynamics," IEEE Trans. Contr. Syst. Tech., 23(1), pp. 389-396, 2015.

[13] Cao, Y., D. Stuart, W. Ren and Z. Meng, "Distributed Containment Control for Multiple Autonomous Vehicles with Double-Integrator Dynamics: Algorithms and Experiments," IEEE Trans. Contr. Syst. Tech., 19(4), pp. 929-938, 2011.

[14] Carona, R., A.P. Aguiar, and J. Gaspar, "Control of Unicycle Type Robots Tracking, Path Following and Point Stabilization," Proc. Intl. Conf. IV Electr. Telecomm., pp. 180-185, Lisbon, Portugal, 2008.

[15] Cheah, C. C., S. P. Hou, and J. J. E. Slotine, "Region-based shape control for a swarm of robots," Automatica, vol. 45, no. 10, pp. 2406–2411, Oct. 2009.

[16] Chen, G., and F.L. Lewis, "Distributed Adaptive Tracking Control for Synchronization of Unknown Networked Lagrangian Systems," IEEE Trans. Syst. Man Cybern. - Part B, 41(3), pp. 805-816, 2011.

[17] Chen, J., D. Sun, J. Yang and H. Chen, "Leader-Follower Formation Control of Multiple Non-Holonomic Mobile Robots Incorporating a Receding-Horizon Scheme," Intl. J. Rob. Res., 29(6), pp. 727-747, 2010.

[18] Chung, F. R. K., Spectral Graph Theory, Providence, RI: Amer. Math. Soc., 1997.

[19] Chung, S.-J., and J.-J. Slotine, "Cooperative Robot Control and Concurrent Synchronization of Lagrangian Systems," IEEE Trans. Rob., 25(3), pp. 686-700, 2009.

[20] Deghat, M., B.D.O. Anderson, and Z. Lin, "Combined Flocking and Distance-Based Shape Control of Multi-Agent Formations," IEEE Trans. Autom. Contr., 61(7), pp. 1824-1837, 2016.

[21] Desai, J.P., J.P. Ostrowski, and V. Kumar, "Modeling and Control of Formations of Nonholonomic Mobile Robots," IEEE Trans. Rob. Autom., 17(6), pp. 905-908, 2001.

[22] De Luca, A., G. Oriolo, and C. Samson, "Feedback Control of a Nonholonomic Car-like Robot," in Robot Motion Planning and Control (J.-P. Laumond, editor), Berlin, Germany: Springer-Verlag, 1998.

[23] Dimarogonas, D.V. and K. H. Johansson, "Further Results on the Stability of Distance-based Multi-robot Formations," Proc. American Contr. Conf., pp. 2972-2977, St. Louis, MO, 2009.

[24] Dimarogonas, D.V. and K.J. Kyriakopoulos, "A Connection Between Formation Infeasibility and Velocity Alignment in Kinematic Multi-Agent Systems," Automatica, 44(10), pp. 2648-2654, 2008.

[25] Dixon, W.E., D. M. Dawson, E. Zergeroglu and A. Behal, Nonlinear Control of Wheeled Mobile Robots, Springer, London, 2001.

[26] Do, K.D., and J. Pan, "Nonlinear Formation Control of Unicycle-Type Mobile Robots," Robot. Autonom. Syst., 55(3),pp. 191-204, 2007.

[27] Dong, W., and J.A. Farrell, "Cooperative Control of Multiple Nonholonomic Mobile Agents," IEEE Trans. Autom. Contr., 53(6), pp. 1434-1448, 2008.

[28] Dong, W., and J.A. Farrell, "Decentralized Cooperative Control of Multiple Nonholonomic Dynamic Systems with Uncertainty," Automatica, 45(3), pp. 706-710, 2009.

[29] Dörfler, F., and B. Francis, "Geometric Analysis of the Formation Problem for Autonomous Robots," IEEE Trans. Autom. Contr., 55(10), pp. 2379-2384, 2010.

[30] Gazi, V. and K.M. Passino, *Swarm stability and optimization*, Springer, Berlin, 2011.

[31] Gazi, V., B. Fidan, R. Ordóñez and M.I. Köksal, "A Target Tracking Approach for Nonholonomic Agents Based on Artificial potentials and Sliding Model Control," ASME J. Dyn. Syst. Measur. Contr., 134(11), Paper 061004, 2012.

[32] Godsil, C., and G. Royle, Algebraic Graph Theory. New York: Springer-Verlag, 2001.

[33] Graver, J., B. Servatius, and H. Servatius. Combinatorial Rigidity. American Mathematical Society. Providence, RI, 1993.

[34] Han, Z., L. Wang, Z. Lin, and R. Zheng, "Formation Control with Size Scaling via a Complex Laplacian-Based Approach," IEEE Trans. Cyber., 46(10), pp.2348-2359, 2016.

[35] Hong, Y., J. Hu, and L. Gao, "Tracking Control for Multi-agent consensus with an active leader and variable topology," Automatica, vol. 42, pp. 1177-1182, 2006.

[36] Izmestiev, I, Infinitesimal Rigidity of Frameworks and Surfaces. Lectures on Infinitesimal Rigidity. Kyushu University, Japan, 2009.

[37] Jackson, B. Notes on the Rigidity of Graphs. Notes of the Levico Conference, 2007.

[38] Kanayama, Y., Y. Kimura, F. Miyazaki and T. Noguchi, "A Stable Tracking Control Method for an Autonomous Mobile Robot," IEEE Conf. Rob. Autom., pp. 384-389 Cincinnati, OH, USA, 1990.

[39] Khaledyan, M., and M. de Queiroz, "Formation Maneuvering Control of Nonholonomic Multi-Agent Systems," Proc. ASME Dyn. Syst. Contr. Conf., Minneapolis, MN, USA, Paper No. DSCC2016-9616, 2016.

[40] Khalil, H.K., Nonlinear Systems, Prentice Hall, Englewood Cliffs, NJ, 2002.

[41] Khoo, S., L. Xie and Z. Man, "Robust Finite-Time Consensus Tracking Algorithm for Multirobot Systems," IEEE/ASME Trans. Mechatr., 14(2), pp. 219-228, 2009.

[42] Kim, B. and P. Tsiotras, "Controllers for Unicycle-type Wheeled Robots: New Theoretical Results and Experimental Validation," IEEE Trans. Robot. Autom., 18(3), pp. 294-307, 2002.

[43] Kostić, D., S. Adinandra, J. Caarls, N. van de Wouv, and H. Nijmeijer, "Saturated Control of Time-Varying Formations and Trajectory Tracking for Unicycle Multi-Agent Systems," Proc. IEEE Conf. Dec. Contr., pp. 4054-4059, Atlanta, GA, USA, 2010.

[44] Kostić, D., S. Adinandra, J. Caarls and H. Nijmeijer, "Collision-free Motion Coordination of Unicycle Multi-Agent Systems," Proc. Amer. Contr. Conf., pp. 3186-3191, Baltimore, MD, USA, 2010.

[45] Krick, L., M.E. Broucke and B.A. Francis, "Stabilization of Infinitesimally Rigid Formations of Multi-Robot Networks," Intl. J. Contr., 83(3), pp. 423-439, 2009.

[46] Krstić, M., I. Kanellakopoulos, and P. Kokotović, Nonlinear and Adaptive Control Design, New York, NY: John Wiley & Sons, 1995.

[47] Lawson, C.L., and R.J. Hanson, Solving Least Squares Problems, Prentice Hall, Englewood Cliffs, NJ, 1974.

[48] Lee, D., and P.Y. Li, "Passive Decomposition Approach to Formation and Maneuver Control of Multiple Rigid-Bodies," ASME J. Dyn. Syst., Measur., Contr., 129(5), pp. 662-677, 2007.

[49] Liang, Y., and H.-H. Lee, "Decentralized Formation Control and Obstacle Avoidance for Multiple Robots with Nonholonomic Constraints," Proc. Amer. Contr. Conf., pp. 5596-5601, Minneapolis, MN, USA, 2006.

[50] de Marina, H.G., B. Jayawardhana, and M. Cao, "Distributed Rotational and Translational Maneuvering of Rigid Formations and their Applications," IEEE Trans. Rob., 32(3), pp. 684-697, 2016.

[51] Marquez, J.H., Nonlinear Control Systems Analysis and Design, Hoboken, NY: Jhn Wiley & Sons, 2003.

[52] Mastellone, S., D.M. Stipanovic, C.R. Graunke, K.A. Intlekofer and M.W. Spong, "Formation Control and Collision Avoidance for Multi-Agent Non-Holonomic Systems: Theory and Experiments," Intl. J. Robotics Res., 27(1), pp. 107-125, 2008.

[53] Mei, J., W. Ren, and G. Ma, "Distributed Coordinated Tracking with a Dynamic Leader for Multiple Euler-Lagrange Systems," IEEE Trans. Autom. Contr., 56(6), pp. 1415-1421, 2011.

[54] Moshtagh, N., N. Michael, A. Jadbabaie and K. Daniilidis, "Vision-based, Distributed Control Laws for Motion Coordination of Nonholonomic Robots," IEEE Trans. Rob., 25(4), pp. 851-860, 2009.

[55] Narendra, K.S. and A.M. Annaswamy, Stable Adaptive Systems, Dover, Mineola, NY, 2005.

[56] Ögren, P., E. Fiorelli, and N.E. Leonard, "Cooperative Control of Mobile Sensor Networks: Adaptive Gradient Climbing in a Distributed Environment," IEEE Trans. Autom. Contr., 49(8), pp. 1292-1302, 2004.

[57] Oh, K.-K. and H.-S. Ahn, "Distance-Based Control of Cycle-Free Persistent Formations," Proc. IEEE Multi-Conf. Syst. and Control, pp. 816-821, Denver, CO, 2011.

[58] Olfati-Saber, A., "Flocking for Multi-agent Dynamic Systems: Algorithm and Theory," IEEE Trans. Autom. Contr., 51(3), pp. 401-420, 2006.

[59] Paige, C.C. and Z. Strakoš, Bounds for the Least Squares Residual Using Scaled Total Least Squares. In: Van Huffel S., Lemmerling P. (eds) Total Least Squares and Errors-in-Variables Modeling, Springer, Dordrecht, 2002.

[60] Pereira, A.R., L. Hsu, and R. Ortega, "Globally Stable Adaptive Formation Control of Euler-Lagrange Agents via Potential Functions," Proc. Amer. Contr. Conf., pp. 2606-2611, St. Louis, MO, USA, 2009.

[61] Pickem, D., L. Wang, P. Glotfelter, Y. Diaz-Mercado, M. Mote, A. Ames, E. Feron, and M. Egerstedt, "Safe, remote-access swarm robotics research on the robotarium," arXiv preprint arXiv:1604.00640, 2016.

[62] Pickem, D., L. Wang, P. Glotfelter, M. Mote, A. Ames, E. Feron, and M. Egerstedt, "The robotarium: a remotely accessible swarm robotics research testbed," arXiv preprint arXiv:1609.04730, 2016.

[63] Qu, Z., Cooperative Control of Dynamical Systems: Applications to Autonomous Vehicles, London, U.K.: Springer-Verlag, 2009.

[64] Ren, W. and R.W. Beard, Distributed Consensus in Multi-vehicle Cooperative Control, London: Springer-Verlag, 2008.

[65] Cao, C. and W. Ren, "Distributed Coordinated Tracking with Reduced Interaction Via a Variable Structure Approach," IEEE Trans. Autom. Contr., 57(1), pp. 33-48, 2012.

[66] Rozenheck, O., S. Zhao, and D. Zelazo, "A Proportional-Integral Controller for Distance Based Formation Tracking," Proc. Europ. Control Conf., pp. 1693-1698, Linz, Austria, 2015.

[67] Sadowska, A., D. Kostić, N. van de Wouw, H. Huijberts and H. Nijmeijer, "Distributed Formation Control of Unicycle Robots," IEEE Conf. Rob. Autom., pp. 1564-1569, Saint Paul, MN, USA, 2012.

[68] Shi, H., L. Wang, and T. Chu, "Flocking of multi-agent systems with a dynamic virtual leader," Int. J. Control, vol. 82, no. 1, pp. 43–58, Jan 2009.

[69] Stilwell, D.J., B.E. Bishop and C.A. Sylvester, "Redundant Manipulator Techniques for Partially Decentralized Path Planning and Control of Platoon of Autonomous Vehicles," IEEE Trans. Syst., Man, and Cybern. - Part B, 35(5), pp. 842-848, 2005.

[70] Summers, T.H., C. Yu, S. Dasgupta, and B.D.O. Anderson, "Control of Minimally Persistent Leader-Remote-Follower and Coleader Formations in the Plane," IEEE Trans. Autom. Contr., 56(12), pp. 2778-2792, 2011.

[71] Sun, D., C. Wang, W. Shang and G. Feng, "A Synchronization Approach to Trajectory Tracking of Multiple Mobile Robots While Maintaining Time-Varying Formations," IEEE Trans. Rob., 25(5), pp. 1074-1086, 2009.

[72] Sun, Z., S. Mou, M. Deghat, and B.D.O. Anderson, "Finite Time Distributed Distance-Constrained Shape Stabilization and Flocking Control for d-Dimensional Undirected Rigid Formations," Intl. J. Rob. Nonl. Contr., 26(13), pp. 2824-2844, 2016.

[73] Sun, Z., B.D.O. Anderson, M. Deghat, and H.-S. Ahn, "Rigid Formation Control of Double-Integrator Systems," Intl. J. Contr., 90(7), pp. 1403-1419, 2017.

[74] Thorvaldsen, C.F.L., and R. Skjetne, 2011, "Formation Control of Fully-Actuated Marine Vessels using Group Agreement Protocols," IEEE Conf. Dec. Contr., pp. 4132-4139, Orlando, FL, USA, 2011.

[75] Yao, J., R. Ordóñez and V. Gazi, "Swarm Tracking Using Artificial Potentials and Sliding Mode Control," ASME J. Dyn. Syst., Meas., Control, 129(5), pp. 749-754, 2007.

[76] Zhang, P., M. de Queiroz, and X. Cai, 2015, "3D Dynamic Formation Control of Multi-Agent Systems using Rigid Graphs," ASME J. Dyn. Syst. Measur. Contr., 137(11), Paper no. 111006, 2015.

[77] Zhao, S., D. Dimarogonas, Z. Sun, and D. Bauso, "A General Approach to Coordination Control of Mobile Agents with Motion Constraints," IEEE Trans. Autom. Contr., in press, DOI: 10.1109/TAC.2017.2750924.

[78] Zhao, X., and T. Huang, "On The Inverse of a General Pentadiagonal Matrix," Appl. Math. and Comp., 202(2), pp. 639-646, 2008.

[79] Zhu, J., J. Lu, and X. Yu, "Flocking of Multi-Agent Nonholonomic Systems with Proximity Graphs," IEEE Trans. Circ. Syst. I, 60(1), pp. 199-210, 2013.

Appendix A. Proof of Matrix K Being Full Column Rank

Here, we prove that K in (3.14) has full column rank by showing that $K^\intercal K \in \mathbb{R}^{2n\times 2n}$ is invertible. First, from (2.8) and (3.9), we have that $P^\intercal P = S^\intercal(\theta_i)\, S(\theta_i) = I_2$ and

$$S^\intercal(\theta_i)S(\theta_j) = S^\intercal(\theta_j)S(\theta_i) = \begin{bmatrix} \cos\theta_{ij} & 0 \\ 0 & 1 \end{bmatrix} \tag{A.1}$$

where $\theta_{ij} = \theta_i - \theta_j$. Using the above properties and the shorthand notation $S_i := S(\theta_i)$, we have that

$$K^\intercal K = \begin{bmatrix} 2I_2 & -S_1^\intercal S_2 & 0_{2\times 2} & 0_{2\times 2} & 0_{2\times 2} & \dots & \dots & 0_{2\times 2} \\ -S_2^\intercal S_1 & 2I_2 & -S_2^\intercal S_3 & 0_2 & 0_{2\times 2} & \dots & \dots & 0_{2\times 2} \\ 0_{2\times 2} & -S_3^\intercal S_2 & 2I_2 & -S_3^\intercal S_4 & 0_{2\times 2} & \dots & \dots & 0_{2\times 2} \\ \vdots & \ddots & \ddots & \ddots & \ddots & \ddots & \ddots & \ddots \\ 0_{2\times 2} & \dots & \dots & \dots & 0_{2\times 2} & -S_{m-1}^\intercal S_{m-2} & 2I_2 & -S_{m-1}^\intercal S_m \\ 0_{2\times 2} & \dots & \dots & \dots & \dots & 0_{2\times 2} & -S_m^\intercal S_{m-1} & I_2 \end{bmatrix}. \tag{A.2}$$

For illustration purposes, for the case of 3 robots, the above matrix becomes

$$K^\intercal K = \begin{bmatrix} 2 & 0 & -\cos\theta_{12} & 0 & 0 & 0 \\ 0 & 2 & 0 & -1 & 0 & 0 \\ -\cos\theta_{12} & 0 & 2 & 0 & -\cos\theta_{23} & 0 \\ 0 & -1 & 0 & 2 & 0 & -1 \\ 0 & 0 & -\cos\theta_{23} & 0 & 1 & 0 \\ 0 & 0 & 0 & -1 & 0 & 1 \end{bmatrix} \tag{A.3}$$

where (A.1) was used.

Interestingly, $K^\intercal K$ is a *pentadiagonal* matrix [3]. Specifically, an $m \times m$ pentadiagonal matrix

Δ has the form

$$\Delta = \begin{bmatrix} a_1 & b_1 & c_1 & 0 & \dots & \dots & \dots & 0 \\ d_2 & a_2 & b_2 & c_2 & 0 & \dots & \dots & 0 \\ e_3 & d_3 & a_3 & b_3 & c_3 & 0 & \dots & 0 \\ 0 & e_4 & d_4 & a_4 & b_4 & c_4 & 0 & \dots \\ \vdots & \ddots & \ddots & \ddots & \ddots & \ddots & \ddots & \ddots \\ 0 & \dots & 0 & e_{m-2} & d_{m-2} & a_{m-2} & b_{m-2} & c_{m-2} \\ 0 & \dots & \dots & 0 & e_{m-1} & d_{m-1} & a_{m-1} & b_{m-1} \\ 0 & \dots & \dots & \dots & 0 & e_m & d_m & a_m \end{bmatrix} \tag{A.4}$$

where $\Delta = [\gamma_{ij}]$ is such that $\gamma_{ij} = 0$ for $|i-j| > 2$.

To find the determinant of Δ, we will utilize the algorithm from [78]: $|\Delta| = \prod_{i=1}^{m} x_i$ if $x_i \neq 0$, $i = 1, \dots, m$ where

$$x_i = \begin{cases} a_1, & i = 1 \\ a_2 - y_1 z_2, & i = 2 \\ a_i - y_{i-1} z_i - \dfrac{e_i c_{i-2}}{x_{i-2}}, & i = 3, \dots, m, \end{cases} \tag{A.5}$$

$$y_i = \begin{cases} b_1, & i = 1 \\ b_i - z_i c_{i-1}, & i = 2, \dots, m-1, \end{cases} \tag{A.6}$$

and

$$z_i = \begin{cases} \dfrac{d_2}{x_1}, & i = 2 \\ \dfrac{d_i - \frac{e_i y_{i-2}}{x_{i-2}}}{x_{i-1}}, & i = 3, \dots, m. \end{cases} \tag{A.7}$$

Note that (A.2) satisfies (A.4) with

$$
\begin{aligned}
&a_1 = \ldots = a_{m-2} = 2, \quad a_{m-1} = a_m = 1 \\
&b_1 = \ldots = b_{m-1} = d_2 = \ldots = d_m = 0 \\
&c_i = \begin{cases} -\cos\theta_{(\frac{i-1}{2})(\frac{i+1}{2})}, & i = \text{odd} \\ -1, & i = \text{even} \end{cases} \\
&e_i = c_{i-2}, \quad i = 3, \ldots, m
\end{aligned} \tag{A.8}
$$

where $m = 2n$, which is obviously even. After substituting (A.8) into (A.5)-(A.7), we obtain the following simplified recursive algorithm

$$
x_i = \begin{cases} 2, & i = 1, 2 \\ a_i - \dfrac{e_i^2}{x_{i-2}}, & i = 3, ..., m. \end{cases} \tag{A.9}
$$

where

$$
e_i^2 = \begin{cases} \cos^2\theta_{(\frac{i-1}{2})(\frac{i+1}{2})}, & i = \text{odd} \\ 1, & i = \text{even}. \end{cases} \tag{A.10}
$$

After some simple calculations, it follows from (A.8)-(A.10) that

$$
\begin{aligned}
x_i &= \begin{cases} 2, & i = 1, 2 \\ 2 - \dfrac{\cos^2\theta_{(\frac{i-1}{2})(\frac{i+1}{2})}}{x_{i-2}}, & i = 3, 5, \ldots, m-3 \\ 1 + \dfrac{2}{i}, & i = 4, 6, , \ldots, m-2 \end{cases} \\
x_{m-1} &= 1 - \frac{\cos^2\theta_{(\frac{m-2}{2})(\frac{m}{2})}}{x_{m-3}} \\
x_m &= \frac{2}{m}.
\end{aligned} \tag{A.11}
$$

From (A.11), it is clear that $x_i \neq 0$ for $i =$ even. Furthermore, we can obtain

$$\begin{aligned} &\frac{i+3}{i+1} \leq x_i \leq 2, \quad i = 1, 3, \ldots, m-3 \\ &\frac{2}{m} \leq x_{m-1} \leq 1, \end{aligned} \tag{A.12}$$

which indicates that $x_i \neq 0$ for $i =$ odd. Since all $x_i \neq 0$, then $|K^\intercal K| = \prod_{i=1}^{m} x_i \neq 0$ and $K^\intercal K$ is invertible. The proof is complete.

Appendix B. Expression for $\dot{\eta}_f$

In this appendix, we compute the expression for $\dot{\eta}_f$. After taking the time derivative of (3.37), we have

$$\begin{aligned}\dot{\eta}_f &= -\frac{d\left(K^{\dagger}(\theta)\right)}{dt}\left[\lambda_2 z + H(\theta_1, t)\right] \\ &\quad -K^{\dagger}(\theta)\left[\lambda_2 \dot{z} + \dot{H}(\theta_1, t)\right].\end{aligned} \tag{B.1}$$

From (3.10) and (3.13), it is obvious that $\dot{z} = K(\theta)\eta + H(\theta_1, t)$. Taking the time derivative of (3.15) yields

$$\dot{H} = \begin{bmatrix} \omega_1 Q R^{\intercal}(\theta_1) S(\theta_{d1})\eta_{d1} + R^{\intercal}(\theta_1)[\omega_{d1} Q^{\intercal} S(\theta_{d1})\eta_{d1} + S(\theta_{d1})\dot{\eta}_{d1}] \\ \omega_{d1} Q^{\intercal} S(\theta_{d1})\eta_{d1} + S(\theta_{d1})\dot{\eta}_{d1} - \omega_{d2} Q^{\intercal} S(\theta_{d2})\eta_{d2} + S(\theta_{d_2})\dot{\eta}_{d2} \\ \vdots \\ \omega_{d(n-1)} Q^{\intercal} S(\theta_{d(n-1)})\eta_{d(n-1)} + S(\theta_{d(n-1)})\dot{\eta}_{d(n-1)} - \omega_{dn} Q^{\intercal} S(\theta_{d_n})\eta_{dn} + S(\theta_{d_n})\dot{\eta}_{dn} \end{bmatrix}$$

where (3.7) and (3.9) were used, and $\dot{\eta}_{d_i}$ is the derivative of the reference signal defined in (3.5).

The derivative of (3.17) is given by

$$\frac{d(K^{\dagger}(\theta))}{dt} = \frac{d\left(K^{\intercal}K\right)^{-1}}{dt} K^{\intercal}(\theta) + \left(K^{\intercal}K\right)^{-1} \dot{K}^{\intercal}(\theta) \tag{B.2}$$

where from (3.14)

$$\dot{K}(\theta) = \Lambda \Upsilon, \tag{B.3}$$

$$\Lambda = \begin{bmatrix} 0_{3\times3} & 0_{3\times3} & 0_{3\times3} & 0_{3\times3} & \cdots & 0_{3\times3} \\ 0_{3\times3} & Q^{\intercal} & 0_{3\times3} & 0_{3\times3} & \cdots & 0_{3\times3} \\ 0_{3\times3} & 0_{3\times3} & Q^{\intercal} & 0_{3\times3} & \cdots & 0_{3\times3} \\ \ddots & \ddots & \ddots & \ddots & \ddots & \ddots \\ 0_{3\times3} & \cdots & \cdots & \cdots & 0_{3\times3} & Q^{\intercal} \end{bmatrix} \in \mathbb{R}^{3n\times3n}, \tag{B.4}$$

$$\Upsilon = \begin{bmatrix} 0_{3\times2} & 0_{3\times2} & 0_{3\times2} & 0_{3\times2} & \cdots & 0_{3\times2} \\ -\omega_1 S(\theta_1) & \omega_2 S(\theta_2) & 0_{3\times2} & 0_{3\times2} & \cdots & 0_{3\times2} \\ 0_{3\times2} & -\omega_2 S(\theta_2) & \omega_3 S(\theta_3) & 0_{3\times2} & \cdots & 0_{3\times2} \\ 0_{3\times2} & 0_{3\times2} & -\omega_3 S(\theta_3) & \omega_4 S(\theta_4) & 0_{3\times2} & 0_{3\times2} \\ \ddots & \ddots & \ddots & \ddots & \ddots & \ddots \\ 0_{3\times2} & \cdots & \cdots & 0_{3\times2} & -\omega_{n-1} S(\theta_{n-1}) & \omega_n S(\theta_n) \end{bmatrix} \in \mathbb{R}^{3n\times2n}, \quad \text{(B.5)}$$

and Q was defined in (3.9). Since for any invertible matrix A,

$$\frac{dA^{-1}}{dt} = -A^{-1}\dot{A}A^{-1}, \quad \text{(B.6)}$$

we have that

$$\begin{aligned} \frac{d\left(K^\intercal K\right)^{-1}}{dt} &= -\left(K^\intercal K\right)^{-1}\left[\dot{K}^\intercal(\theta)\,K(\theta) + K^\intercal(\theta)\dot{K}(\theta)\right] \\ &\quad \times\left(K^\intercal K\right)^{-1}. \end{aligned} \quad \text{(B.7)}$$

From the above equations, we can see that the expression for $\dot{\eta}_f$ is dependent on the following variables: θ (through trigonometric functions), η, z, and t.

Vita

Milad Khaledyan was born and raised in Kurdistan, Iran. Before coming to LSU, he received a B.Sc. degree in Aerospace Engineering from Sharif University of Technology, Tehran, Iran, in 2014. During that time, he worked on several research projects on linear control. He joined the Mechanical Engineering Ph.D. program at LSU under the supervision of Dr. Marcio de Queiroz in August 2014. He has been working at LSU as an instructor/teaching assistant in several courses such as System Dynamics and Modeling, Dynamics, and Mechanical Design. His research interests focus on nonlinear control systems with application to cooperative behavior of nonholonomic multi-agent systems. He plans to complete his doctoral studies in August 2018.